NGU REPORT 2021.017

Processing and interpretation of Magnetic and Gravity
data from Brattbakken, Verdal municipality, Trøndelag County

GEOLOGY FOR SOCIETY

SINCE 1858

GEOLOGICAL SURVEY OF NORWAY

- NGU -

NGU REPORT
2021.017

Processing and interpretation of Magnetic and Gravity data from Brattbakken, Verdal municipality, Trøndelag County

NORGES GEOLOGISKE UNDERSØKELSE
- NGU -

Geological Survey of Norway
P.O.Box 6315 TORGARDEN
NO-7491 TRONDHEIM
Tel.: 47 73 90 40 00

REPORT

Report no.: 2021.017

ISSN: 0800-3416 (print)
ISSN: 2387-3515 (online)

Grading: Open

Title:
Processing and interpretation of Magnetic and Gravity data from Brattbakken, Verdal municipality, Trøndelag county

Authors:
Frida Mathayo Mrope, Jomar Gellein, Jan Sverre Sandstad, Lars Petter Nilsson, Hanne-Kristin Paulsen and Victor Mapuranga*

Client:
NGU

County:
Trøndelag

Municipality:
Verdal

Map-sheet name (M=1:250.000)
Østersund

Map-sheet no. and -name (M=1:50.000)
Vera 1822-4

Deposit name and grid-reference:
WGS84, UTM 33N 369580E, 7092895N

Number of pages: 54 **Price (NOK): 215**
Map enclosures:

Fieldwork carried out:	**Date of report:**	**Project no.:**	**Person responsible:**
09.09 -14.09.2020	November 2022	386900	Marco Brönner

Summary:
This report describes data processing and interpretation of magnetic and gravity data acquired in Brattbakken area, Verdal, Trøndelag county. The survey was carried out in September 2020. This work is part of the project named NIKKEL I TRØNDELAG, a project aiming at understanding the lateral and vertical extents of the nickel deposits in Trøndelag region.

The interpretation was carried out by incorporating 3D VOXI inversion of magnetic data and 2D forward modelling of the magnetic and gravity data. The areal geology indicates the presence of Gula group dominating the survey area. The group is comprised of Gula schist intercalated with Gula amphibolite and banded iron formation (BIF). The Gula group, namely the amphibolite is intruded by gabbro and pyroxenite. The south-eastern part of the survey area is covered by Funnsjø greenstone.

The results from 3D inversion and 2D modelling suggest the intrusions to be about 215 – 260 m wide and 90 -270 m thick.

The ore zone within the pyroxenite intrusion was further examined. An inversion with denser grid cell size was carried out. The interpreted result suggests the identified ore prospect to be between 20 - 30 m thick with susceptibility of 0.12 SI. However, there is a potential for significant larger thickness and up to 145 m with varying susceptibility from 0.06 SI to 0.12 SI across the prospect area. The variation of susceptibility values could indicate varying ore grades or that some anomalies are caused by other high magnetic sources.

Keywords:	**Magnetic**	**Gravity**
Processing	**2D modelling**	**VOXI 3D Inversion**
	Interpretation	**Technical report**

CONTENTS

1. INTRODUCTION 10
1.1 Project objective 10
1.2 Report outline 11
2. SURVEY SPECIFICATIONS 11
2.1 Gravity and Magnetic Measurements 11
2.2 Survey layout 12
3. DATA PROCESSING AND PRESENTATION 13
3.1 Total Field Magnetic Data 13
3.2 Gravity Data 17
4. 2D MODELLING OF MAGNETIC AND GRAVITY DATA 21
5. VOXI 3D INVERSION OF MAGNETIC DATA 25
5.1 VOXI 3D inversion of synthetic data 25
5.2 VOXI 3D inversion of real data 31
5.3 Revised 2D models based on 3D inversion results. 36
5.4 VOXI 3D inversion of the nickel prospect area 39
6. DATA INTERPRETATION AT THE PROSPECT AREA 42
7. CONCLUSION 47
8. REFERENCES 48
9. APPENDIX 49
Appendix A1: Maps of magnetic anomalies 49
Appendix A2: 2D models down to 14 km deep. 53

FIGURES

Figure 1: Survey location (red rectangle) showing two gravity profiles (in blue). 10
Figure 2: Aerial photo of the area of interest with magnetic (red) and gravity (blue) survey layout. The cyan coloured boxes mark the prospect area. 12
Figure 3: Total field magnetic anomaly at 30% transparent over a relief map. The magnetic profile is shown in red while gravity profiles L1 and L2 are in blue. The box marks the prospect area. 14
Figure 4: y-Horizontal gradient at 30% transparent over a relief map. The magnetic profile is shown in red, gravity profiles L1 and L2 are in blue. The box marks the prospect area. 15
Figure 5: Magnetic anomaly of airborne data at 30% transparent over a relief map. The black lines show the helicopter flight lines compared to the gravity profiles L1 and L2 in blue. The box marks the prospect area. 16
Figure 6: Complete Bouguer anomaly at 30% transparent over a relief map. The gravity profiles L1 and L2 are shown in blue. The box marks the prospect area. Dashed circles highlight local anomalies standing out of the regional trend. 19
Figure 7: A complete Bouguer anomaly from available regional gravity data displayed at 30% transparent over a relief map. Blue crosses are regional gravity stations and the local gravity profiles L1 and L2 are shown at the centre of the map. The data indicates an increased rock density towards south-east ends of profiles L1 and L2. 20
Figure 8: Location of the petrophysical and geological data in the survey area. The gravity profiles L1 and L2 are shown in blue. The boxes mark the prospect area. Purple lines demarcate lithological units (Nilsson et al.,2021). 21
Figure 9: A 2D profile along the western line L1. Triangles on the surface are locations of gravity stations (black) and magnetic data points (grey). The gravity and magnetic profiles in the middle show the calculated data (solid lines) fitting the observed data (dots). The plan view is taken at (-)750 m above msl. 23
Figure 10: A 2D profile along the eastern line L2. Triangles on the surface are locations of gravity stations (black) and magnetic data points (grey). The gravity and magnetic profiles in the middle show the calculated data (solid lines) fitting the observed data (dots). The plan view is taken at (-)750 m above msl. 24
Figure 11: A 2D section of the synthetic model along line L1. Triangles on the surface of the model are locations of gravity stations (black) and magnetic data points (grey). 25
Figure 12: A 3D view of the model showing the target, susceptibility >0.005 SI. 26
Figure 13: Synthetic data from the 3D geo-model. Black lines are location of gravity profiles L1 and L2. 26

Figure 14: Unconstrained inversion results of synthetic data shown along line L1. Triangles on the surface are locations of gravity stations (black) and magnetic data points (grey). 27
Figure 15: Unconstrained inversion results of synthetic data showing the recovered target and location of line L1. 28
Figure 16: Constrained inversion results. The target is well recovered. 29
Figure 17: Convergence curve of the synthetic data inversion. 30
Figure 18: Calculated data from the inversion result. Black lines are location of gravity profiles L1 and L2. 31
Figure 19. Snåsa airborne data acquired in year 2020. The gravity profiles L1 and L2 are shown in blue. The box marks the prospect area. Helicopter flight lines are in cyan and purple lines demarcate lithological units. 32
Figure 20: A 3D cube of inversion result of airborne data showing susceptibility distribution in x, y, z. Black lines are locations of gravity profiles L1 and L2. 33
Figure 21: 3D inverted model showing a spatial distribution of magnetic anomalies. The gravity profiles L1 and L2 are shown in blue and geological boundaries in purple lines for reference. 34
Figure 22: 3D inversion results showing vertical sections along line L1. Superimposed on the sections (black outlines) are the 2D modelling results for comparison. 35
Figure 23: A vertical section along line L2 from inversion with linear background removal. Superimposed on the section (black outlines) is the 2D modelling results for comparison 36
Figure 24: A revised 2D model (black outlines) along line L1 fitting the VOXI 3D inverted model. 36
Figure 25: A revised 2D model along line L1. The gravity and magnetic profiles show the calculated data (solid lines) fitting the observed data (dots). 37
Figure 26: A revised 2D model along line L2. The gravity and magnetic profiles show the calculated data (solid lines) fitting the observed data (dots). 37
Figure 27: Convergence curve of the real data inversion. 38
Figure 28: Calculated data from the inversion result. This data fits the observed data (Figure 19). The gravity profiles L1 and L2 are shown in blue. The box marks the prospect area. Helicopter flight lines are in cyan and purple lines are lithological demarcations. 38
Figure 29: Measured data (5 m x 5 m grid) at nickel prospect area (Cyan box). The inset image shows the location of the prospect in the survey area. The gravity profile L1 is shown in blue and ground magnetic profiles in red. Geological boundaries are shown in purple. 39
Figure 30: 3D inversion result of the prospect area. Vertical exaggeration = 1. 40

Figure 31: Observed (a) and calculated (b) data from the inversion result. The box marks the prospect area. The gravity profiles L1 is shown in blue and ground magnetic profiles in red. Geological boundaries are in purple. 41
Figure 32: 3D inversion result: Top view at Sucs. > 0.06 SI (Pink), > 0.1 SI (red) and > 0.15 SI (purple). The gravity profile L1 is shown in blue. Geological boundaries are in purple. A-F mark anomalies further explained in the text. 42
Figure 33: 3D inversion result: View from south at Sucs. > 0.06 SI (Pink), > 0.1 SI (red) and > 0.15 SI (purple). Anomalies D and E are smaller and shallower. A-F mark anomalies further explained in the text. 43
Figure 34: 2D modelling of the nickel ore prospect along the western line, LS. (a) 2D profile with a plan view at (-) 823 m above msl. (b) a map view showing the location of line LS and the respective anomalies overlaying the observed data. (c) 3D inverted model superimposed by 2D model outlines for comparison. 44
Figure 35: 2D modelling of the nickel ore prospect along the middle line LN. (a) 2D profile with a plan view at (-) 810 m above msl. (b) a map view showing the location of line LN and the respective anomalies overlaying the observed data. (c) 3D inverted model superimposed by 2D model outlines for comparison. 45
Figure 36: 2D modelling of the nickel ore prospect along the crossing line LX. (a) 2D profile with a plan view at (-) 781 m above msl. (b) a map view showing the location of line LX and the respective anomalies overlaying the observed data. (c) 3D inverted model superimposed by 2D model outlines for comparison. 46
Figure 37: Total Horizontal gradient of the magnetic field at 30% transparent over a relief map. The magnetic profile is shown in red, gravity profiles in blue. The box marks the prospect area. 49
Figure 38: x-Horizontal gradient of the magnetic field at 30% transparent over a relief map. The magnetic profile is shown in red, gravity profiles in blue. The box marks the prospect area. 50
Figure 39: First vertical derivative of the magnetic field at 30% transparent over a relief map. The magnetic profile is shown in red, gravity profiles in blue. The box marks the prospect area. 51
Figure 40: Magnetic Tilt Derivative at 30% transparent over a relief map. The magnetic profile is shown in red, gravity profiles in blue. The box marks the prospect area. 52
Figure 41: 2D full profile along line L1. The gravity and magnetic profiles in the middle show the calculated (solid lines) and observed data (dots). The plan view is at (-)750 m above msl. 53

Figure 42: 2D full profile along line L2. The gravity and magnetic profiles in the middle show the calculated (solid lines) and observed data (dots). The plan view is at (-)750 m above msl. 54

TABLES

Table 1: Density and susceptibility mean values. 22
Table 2: Density and susceptibility values for the ore anomalies 44

1. INTRODUCTION

1.1 Project objective

This report covers data processing and interpretation of magnetic and gravity data acquired in Brattbakken, Verdal municipality in Trøndelag county (Figure 1). This work aims at understanding the lateral and vertical extents of the known nickel occurrences at Skjækerdalen locality at Brattbakken area. The project is part of the project NIKKEL I TRØNDELAG. The survey was carried out in September 2020. The interpretation is based on the analysis of susceptibility and density distribution in the subsurface and its correlation to the surface geology.

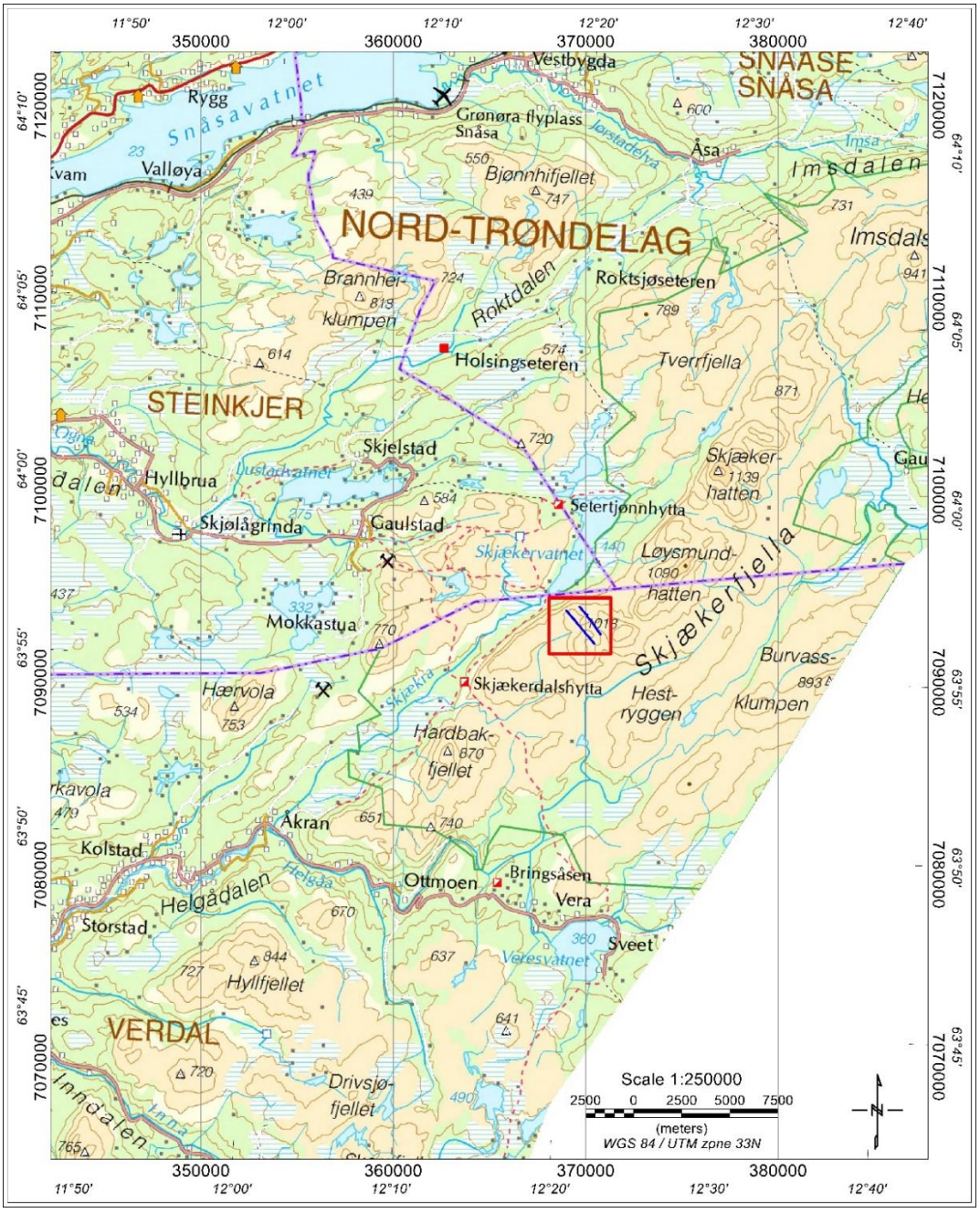

Figure 1: Survey location (red rectangle) showing two gravity profiles (in blue).

Nickel is ferromagnetic and has relatively high density (8908 kg/m^3). The nickel ore will most likely be denser and high in susceptibility compared to the surrounding rocks. These characteristics make gravity and magnetic methods appropriate for its exploration. The survey was planned such that one gravity profile (L1) will cross the ore area and the other line (L2) about 800 m away from line L1 will monitor the ore extent towards northeast. The lines are extended beyond the ore area to map the density of the side rocks and hence observe the contrast. Magnetic profiles were planned to follow the gravity profiles for 2D modelling purposes, and a denser coverage at the ore area for a detailed analysis.

1.2 Report outline

This report presents:

- Processing of magnetic data.
- Processing of gravity data.
- 2D modelling of the magnetic and gravity data along the gravity survey lines.
- 3D inversion of synthetic and real magnetic data.
- Interpretation of the 3D inversion results.
- Conclusions.

2. SURVEY SPECIFICATIONS

2.1 Gravity and Magnetic Measurements

Gravity data were measured along two profiles trending NW-SE (Figure 2). The lines are 2.3 km and 1.8 km long for L1 and L2 respectively. Line spacing is about 800 m. Spacing between the stations vary from 50 m in the prospect area to 350 m for stations away from the prospect area.

Scintrex CG-5 gravimeter with theoretical accuracy of 0.001 mGal (Scintrex 2019) was used for data collection. The sensor elevation and station locations were measured using a differential GPS. Scintrex CG-5 gravimeter is a relative gravimeter measuring the gravity variations between the observation stations. To determine the absolute gravity of the measured area, the measurements were calibrated using the absolute gravity station which is located at NGU's office. For time drift control, a specific point was selected at the survey area where gravity measurements were done in the morning and evening of the survey dates. Topcon Legacy E (TopCon 2019) with accuracy better than 10 cm was used for positioning of both base station and observation stations.

The magnetic data were acquired surrounding the two gravity lines (Figure 2) but not exactly on the gravity profiles. The data was collected using GEM GSM -19 magnetometer with theoretical accuracy of ± 0.2 nT. The magnetometer and GPS were mounted on a backpack and data was collected whilst walking.

2.2 Survey layout

The survey layout is shown in Figure 2. It is comprised of magnetic profiles (red) and gravity profiles (blue lines). 29 gravimeter stations (blue circles) are arrayed in two NW-SE lines. Line L1, the westernmost line has 17 stations and line L2 has 12 stations. At the central west of line L1 is the known nickel prospect with an area of interest highlighted by a cyan coloured rectangle (195 m x 125 m). The smaller, inner cyan rectangle highlights a location where five outcrop samples were identified as nickel ore with very high susceptibility values. One of the five samples was classified as an insitu outcrop.

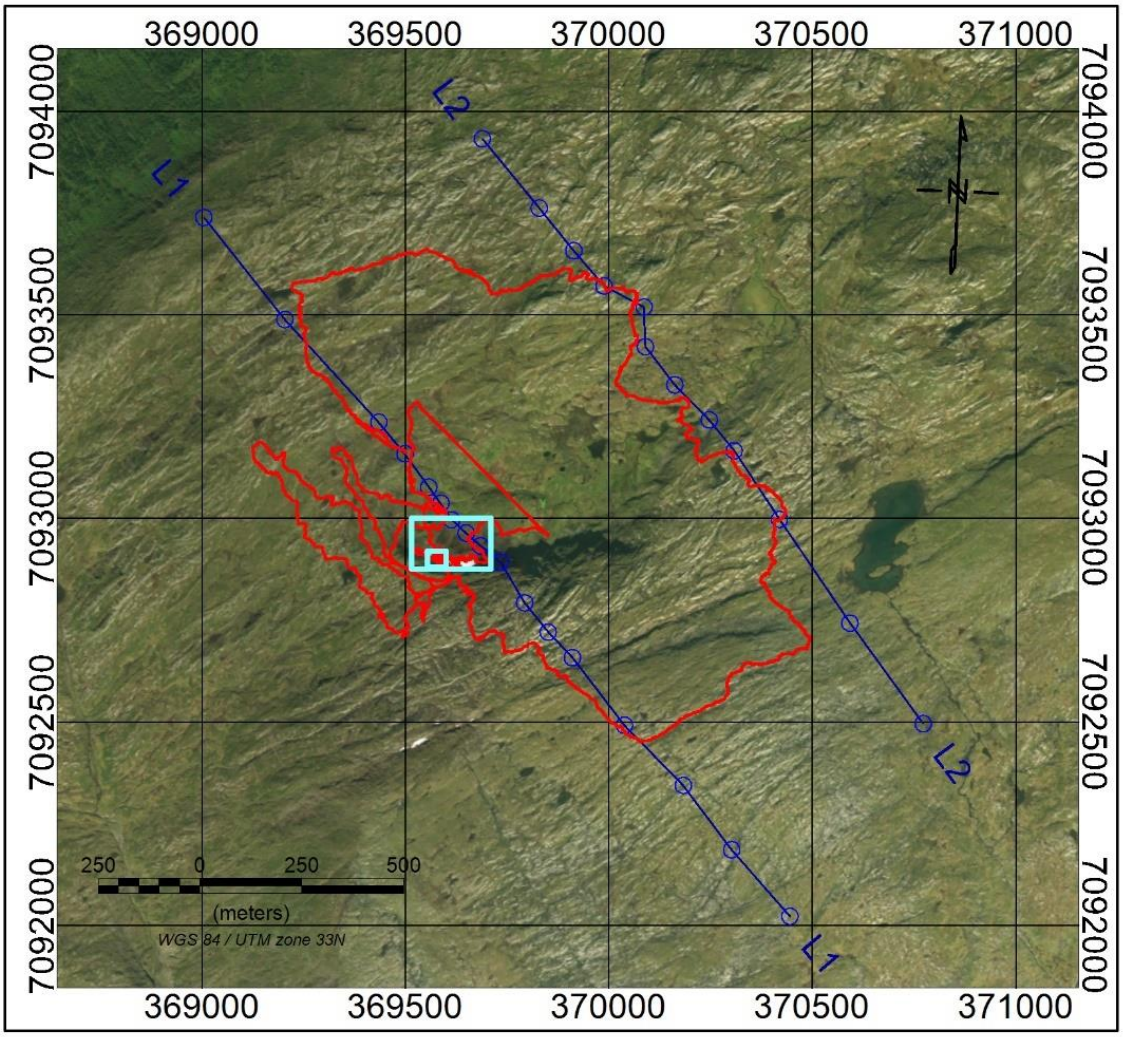

Figure 2: Aerial photo of the area of interest with magnetic (red) and gravity (blue) survey layout. The cyan coloured boxes mark the prospect area.

3. DATA PROCESSING AND PRESENTATION

The gravity data were collected and processed by Jomar Gellein. The magnetic data were collected by Jan Sverre Sandstad and processed by Frida Mathayo Mrope. Frida also did the 2D modelling and VOXI 3D inversion of the data. VOXI inversion results were reviewed by Victor Mapuranga, a Customer Solutions Specialist at Seequent. The interpretation work was done in collaboration with the field geologists: Jan Sverre Sandstad, Hanne-Kristin Paulsen and Lars Petter Nilsson who is also the project leader.

3.1 Total Field Magnetic Data

At the first stage the raw magnetic data was visually inspected, and spikes were removed manually. Non-linear filter was applied to the raw data to eliminate short-period spikes. Typically, diurnal correction is applied to magnetic data before gridding.

Diurnal Corrections

The temporal fluctuations in the magnetic field of the earth affect the total magnetic field recorded during the survey period. This is commonly referred to as the magnetic diurnal variation. These fluctuations can be effectively removed from the magnetic dataset by using a stationary reference magnetometer that records the magnetic field of the earth simultaneously while measuring the magnetic data at a given area. Changes in magnetic field recorded at a stationary magnetometer is related to the diurnal effect. During this survey, the second magnetometer for stationary reference was not available. Because the survey period was very short, the influence of diurnal variations was deemed negligible. Therefore, diurnal correction was not applied to the data.

Magnetic data processing, gridding, and presentation

The total field magnetic anomaly data ($\mathbf{B}_{TA}$) were calculated from the total field data ($\boldsymbol{B}_{Tf}$) after subtracting the International Geomagnetic Reference Field (IGRF) model for the surveyed area (equation 3-1)

$$B_{TA} = B_{Tf} - IGRF \qquad 3\text{-}1$$

IGRF 2020 model was employed in these calculations to deduct the magnetic field resulting from the earth's core.

The total field anomaly data were corrected for RTP (reduced to pole) before gridding at 50 m x 50 m cell size using a minimum curvature gridding algorithm. A resulting grid is shown in Figure 3.

The processing steps of magnetic data presented so far, were performed on point basis. The following steps are performed on grid basis.

The horizontal and vertical gradient along with the tilt derivative of the total magnetic anomaly were calculated from the total magnetic anomaly grid. The magnitudes of the horizontal and vertical gradients were calculated according to equations (3-2) and (3-3) respectively.

$$HG = \sqrt{\left(\frac{\partial(B_{TA})}{\partial x}\right)^2 + \left(\frac{\partial(B_{TA})}{\partial y}\right)^2} \qquad 3\text{-}2$$

$$VG = \left(\frac{\partial(B_{TA})}{\partial z}\right) \qquad 3\text{-}3$$

where: $\mathbf{B}_{TA}$ is the total field anomaly (RTP corrected). The tilt derivative (TDR) was calculated according to equation (3-4)

$$TDR = tan^{-1}\left(\frac{VG}{HG}\right) \qquad 3\text{-}4$$

Figure 3 shows the map of Total field magnetic anomaly (RTP). The map of the calculated y-horizontal gradient is shown in Figure 4 and the rest of the maps are shown in appendix A1.

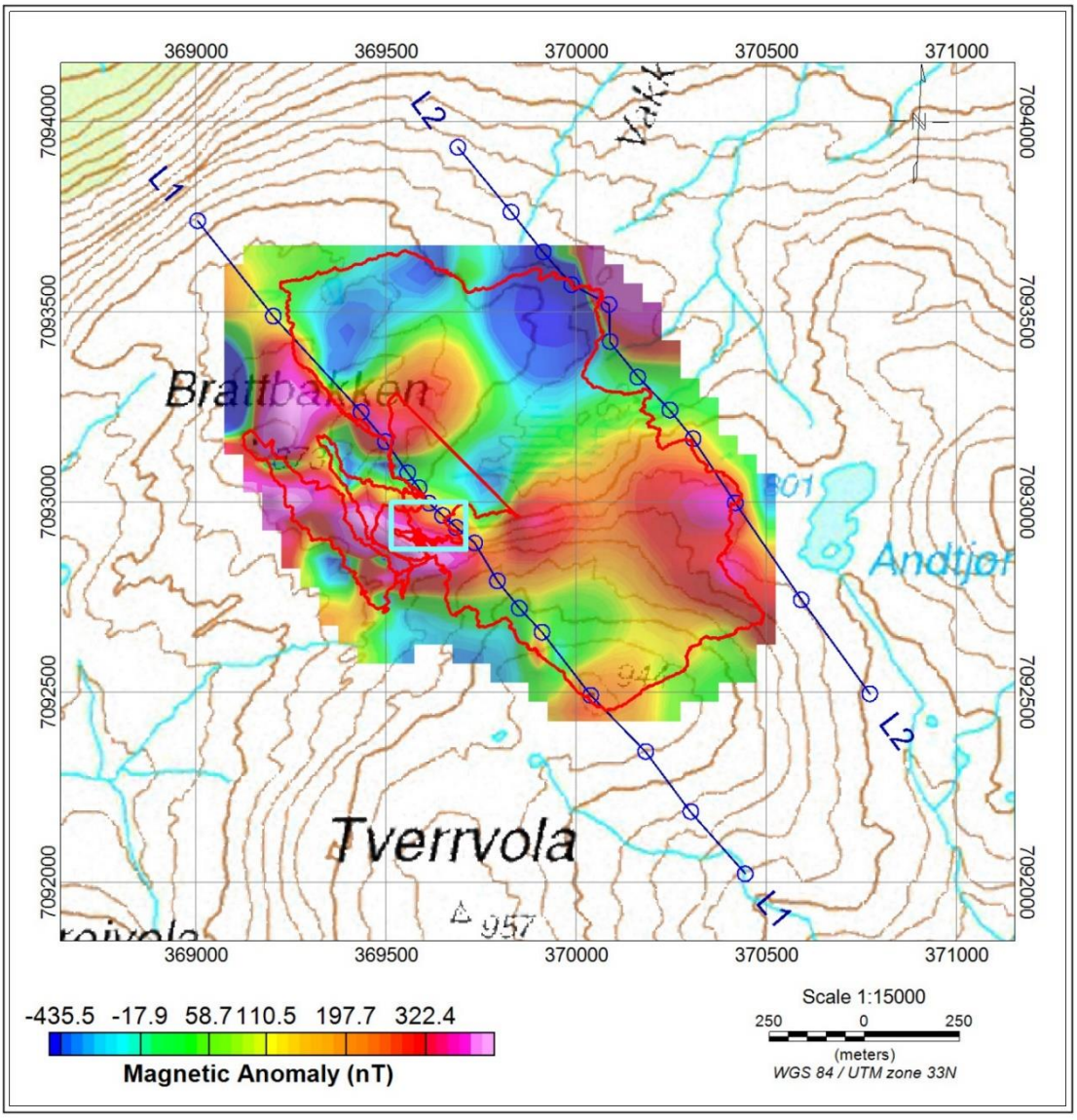

Figure 3: Total field magnetic anomaly at 30% transparent over a relief map. The magnetic profile is shown in red while gravity profiles L1 and L2 are in blue. The box marks the prospect area.

The anomaly maps represent the distribution of magnetization over the surveyed area. Figure 3 shows several positive anomalies in the area including at the prospect region. A stronger anomaly is mapped in the vicinity of the area of interest and is connected to the prospect location. Looking at the derivates, in Figure 4, the y-horizontal gradient displays a negative gradient at the prospect area. This attribute isolates the prospect from the high magnetic body in the south-western side.

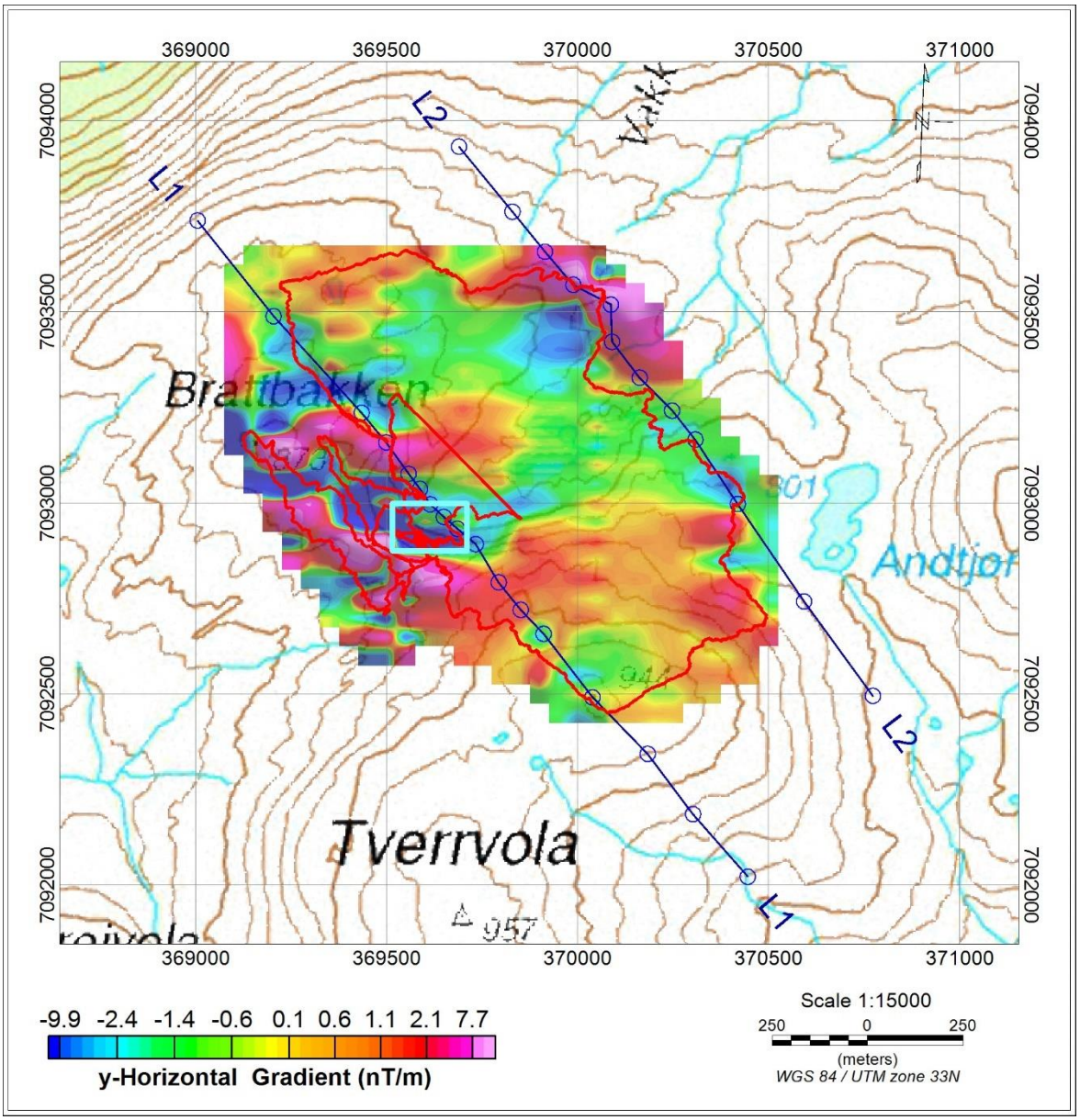

Figure 4: y-Horizontal gradient at 30% transparent over a relief map. The magnetic profile is shown in red, gravity profiles L1 and L2 are in blue. The box marks the prospect area.

It is important to note that the magnetic profiles parallel to the gravity lines are about 800 m apart. The wide separation makes the magnetic information in-between the profiles unreliable on a 50 m x 50 m grid and therefore, interpretation in that area must be handled with care. However, there is a good data coverage within the prospect area.

The survey area is also covered by airborne data (Figure 5) which was collected in year 2020 (Verdal and Snåsa) at 200 m line spacing (Ofstad et al., 2021). The presented anomaly map is from a 50 m x 50 m grid and displayed with the same colour scale as ground magnetic data in Figure 3 for comparison. Because of higher sensor elevation (average 55 m above the ground), anomalies in the airborne data are observed to be weaker in magnitude. However, due to its relatively dense spacing it has a better delineation of anomalies. Strong anomalies observed on airborne data can also be observed on ground data where coverage is substantial.

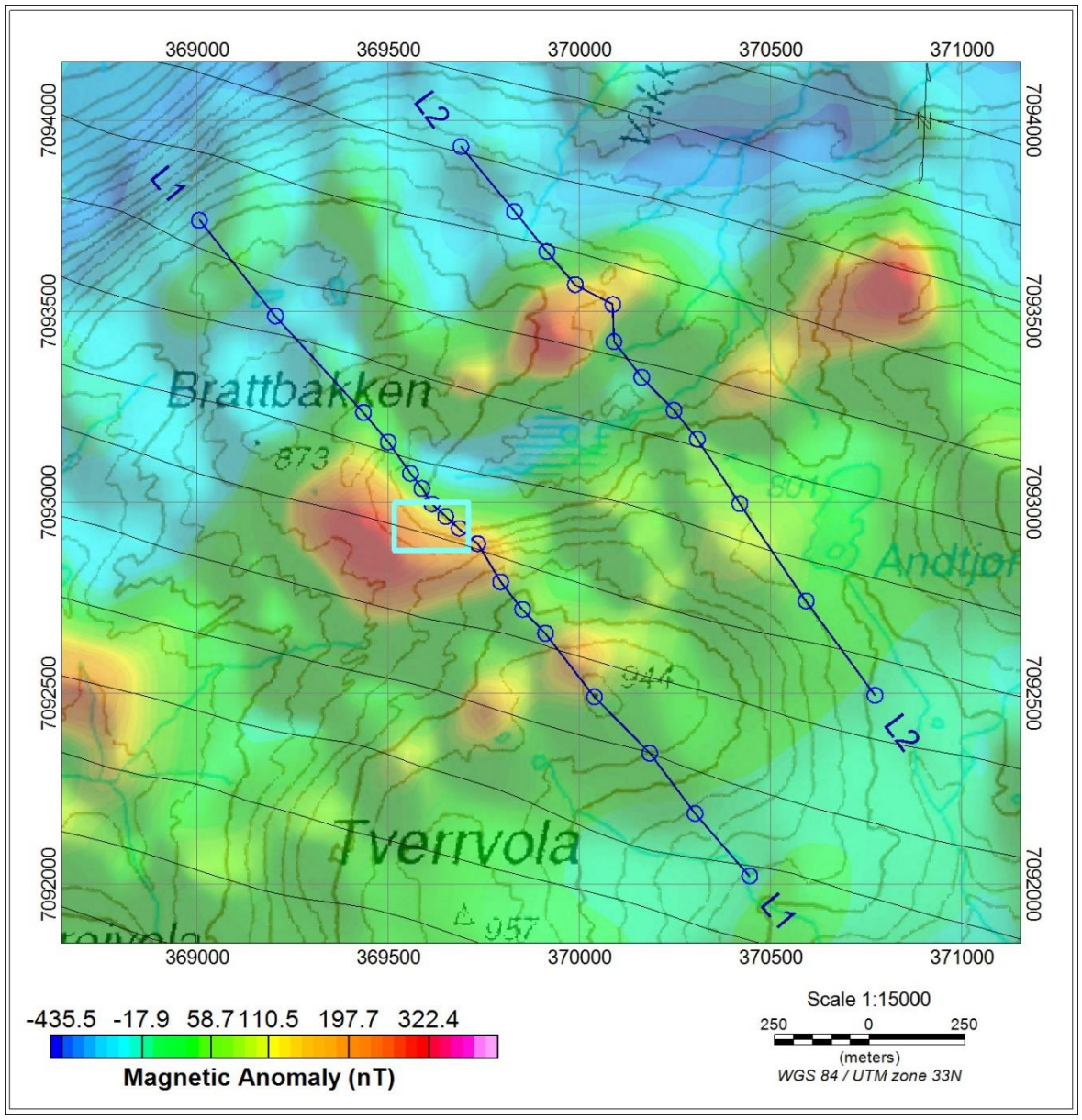

Figure 5: Magnetic anomaly of airborne data at 30% transparent over a relief map. The black lines show the helicopter flight lines compared to the gravity profiles L1 and L2 in blue. The box marks the prospect area.

Blue circles on Figure 5 are gravity stations along two lines. Airborne survey lines (black) are 200 m apart in WNW-ESE orientation. The nickel prospect area is highlighted by a cyan rectangle, 195 m x125 m.

3.2 Gravity Data

Processing of the measured gravity data involves several corrections to ensure that the gravity readings are only influenced by a response from rock densities in the subsurface. This dataset was processed using Geosoft, Oasis montaj Version 9.7.1. Gravity and Terrain Correction, Geosoft Inc. (2018). Corrections applied on this data are:

- Earth tide correction - to account for the earth tides due to the position of the sun and the moon at the time and location of data collection.
- Instrument height correction - to account for the effect of the instrument elevation above the ground.
- Drift correction – corrects for the differences observed on the measured data at a fixed location. It is a linear drift over time.
- Absolute gravity calibration.

Gravity reduction of the measured and corrected data (g_{obs}) is a necessary step to calculate gravity anomalies to identify density distribution of the underlying rocks. Components of gravity reduction include:

- Latitude correction to account for the earth's rotation and earth's elliptical shape, that the distance to the earth's centre of mass is different at different latitudes. The latitude correction (g_n) is given by equation 3-5 below. The observed data is corrected by subtracting this factor.

$$gn = 978031.85\left(1.0 + 0.005278895\,sin^2(lat) + 0.000023462\,sin^4(lat)\right) \quad (mGal) \qquad 3\text{-}5$$

where *lat* is the latitude.

- Free air gravity anomaly calculation – It considers the weakening of field strength for measurements taken at elevations higher than sea level. It corrects for gravity variations caused by elevation differences of the measuring stations. Free air corrected anomaly (g_{fa}) is defined as:

$$gfa = gobs - gn + 0.3086h \quad (mGal) \qquad 3\text{-}6$$

where *h* is the instrument elevation above mean sea level.

- Bouguer anomaly calculation – It corrects the free air gravity anomaly to account for gravitational attraction of rock masses between the measurement point and the sea level. It seeks to reduce the data to obtain the sea level equivalent. The Bouguer anomaly (g_b) is given by:

$$gb = gfa - 0.0419088 * [D * Hs + (Dw - D) * Hw + (Di - Dw) * Hi] - Gc\ (mGal) \qquad 3\text{-}7$$

where D and H_s are Bouguer density of the earth (2.67 g/cm^3) and station height respectively, D_w and H_w are density of water and water depth and Di and Hi are density of ice and ice thickness, respectively. The densities are in g/cm^3, and heights/depth are in meters. Gc is curvature correction.

- Terrain correction (T_C) – to account for variations in the observed data caused by irregularities of the earth topography near each measurement station. Terrain corrected Bouguer anomaly also referred as complete Bouguer gravity anomaly (g_{bc}) is calculated as:

$$gbc = gb + Tc \quad (mGal) \qquad 3\text{-}8$$

The absolute gravity calibration, gravity corrections and anomaly calculations were done with reference to The International Gravity Standardization net 1971 (IGSN71) system.

Figure 6 displays the complete Bouguer anomaly of the survey area corresponding to the density distribution over the area. Data was gridded at 50 m x 50 m using minimum curvature gridding algorithm. The results indicate a general increase of rock density towards southeast. Two localised anomalies can be identified on the map (dashed circles). The line separation is about 800 m leading to a large area of interpolation in-between the profiles.

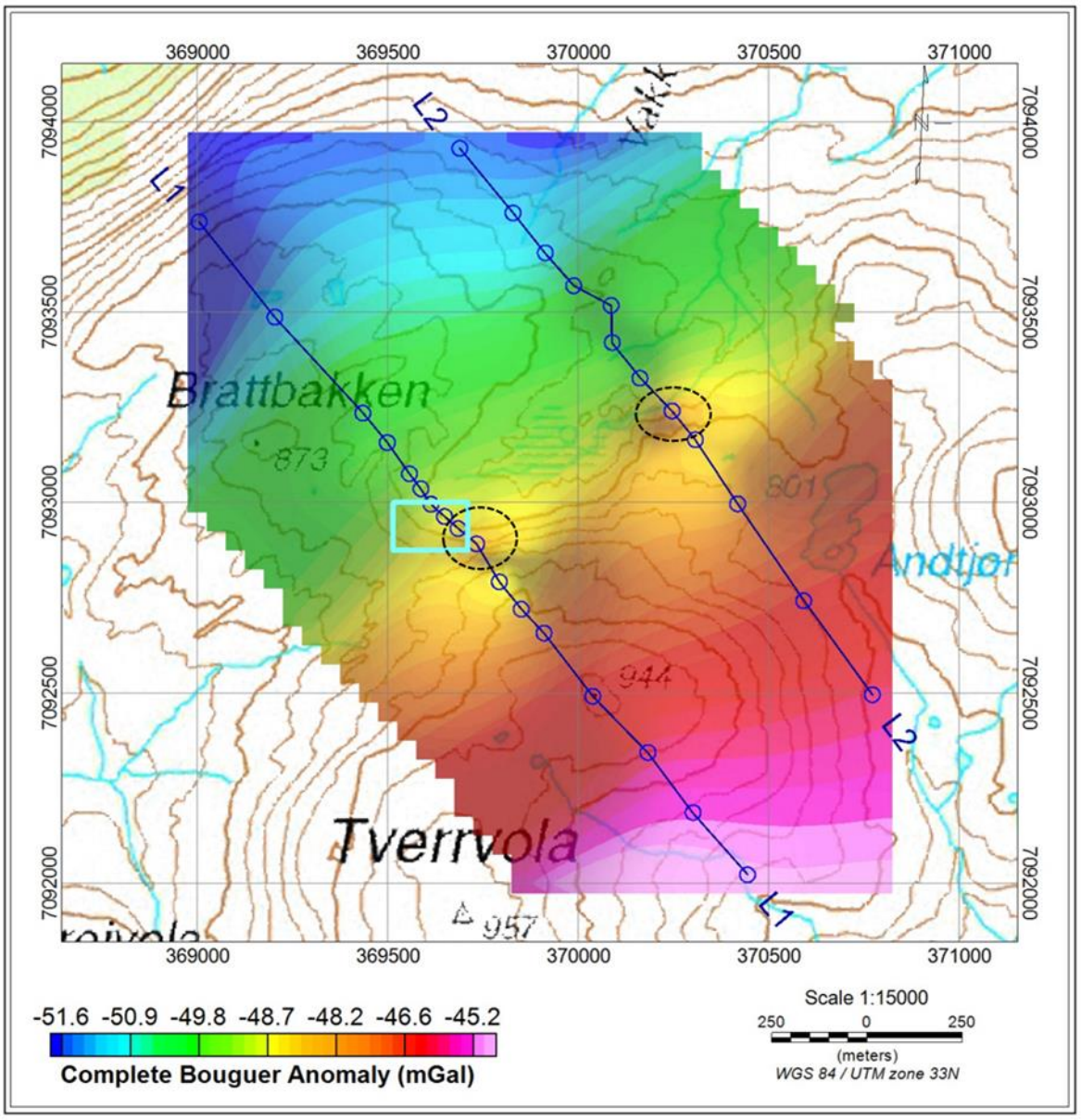

Figure 6: Complete Bouguer anomaly at 30% transparent over a relief map. The gravity profiles L1 and L2 are shown in blue. The box marks the prospect area. Dashed circles highlight local anomalies standing out of the regional trend.

Gravity data from regional surveys for this area is available at NGU database. Figure 7 displays a regional gravity anomaly from sparsely located stations (blue crosses). The data is complete Bouguer anomaly gridded at 500 m cell size using minimum curvature gridding algorithm. The regional trend is similar to that observed on the local survey (Figure 6).

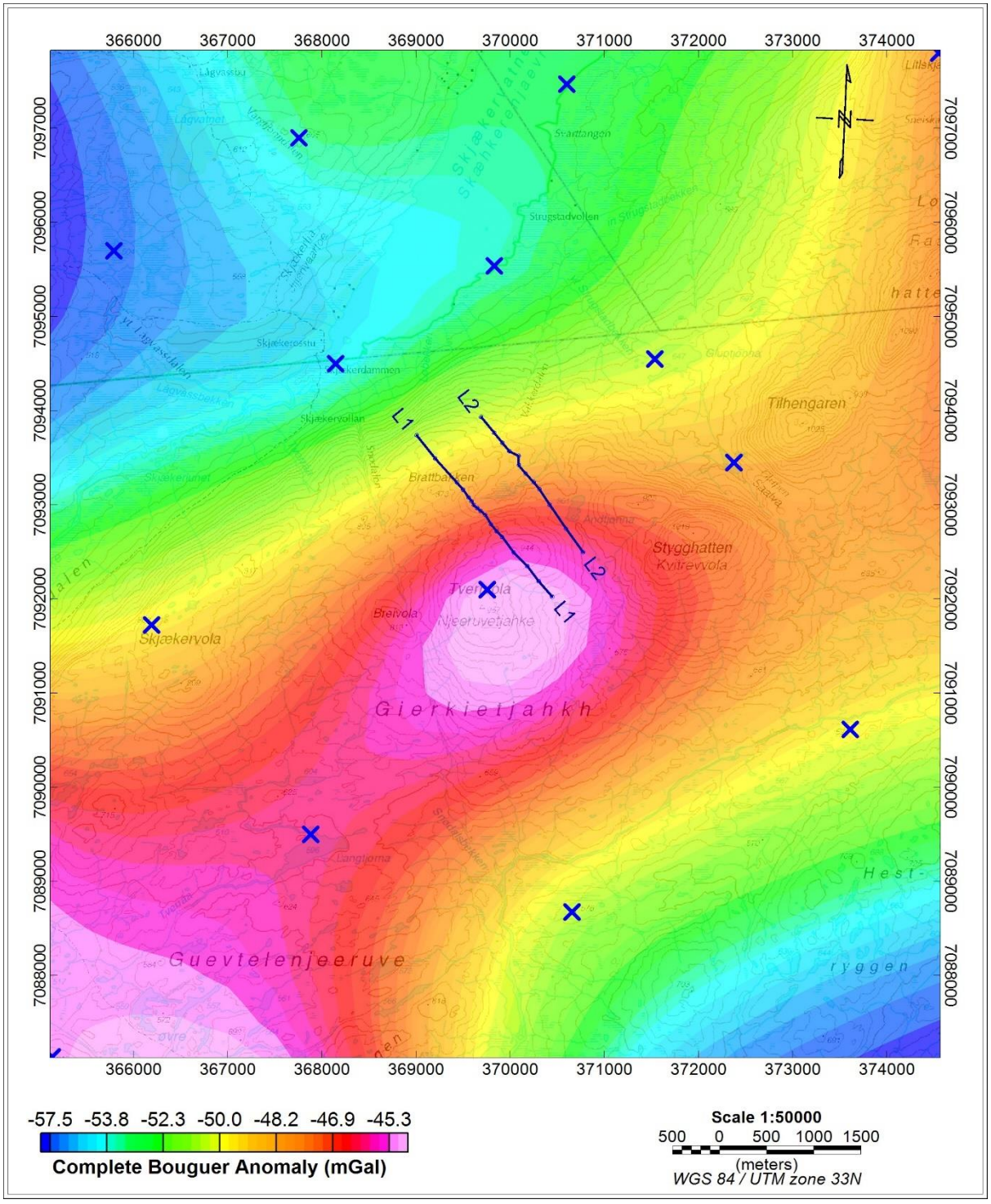

Figure 7: A complete Bouguer anomaly from available regional gravity data displayed at 30% transparent over a relief map. Blue crosses are regional gravity stations and the local gravity profiles L1 and L2 are shown at the centre of the map. The data indicates an increased rock density towards south-east ends of profiles L1 and L2.

4. 2D MODELLING OF MAGNETIC AND GRAVITY DATA

The interpretation process involved 2D forward modelling of the gravity and magnetic data along two gravity profiles, L1 and L2 as shown in Figure 8. The modelling was done using GM-SYS 2D modelling software by Oasis Montaj (Geosoft 9.8.1). The software can run simultaneous forward modelling of gravity and magnetic data. Therefore, 2D forward modelling provides a model which has both, density, and susceptibility information. The available information regarding the geology of the area was incorporated in the modelling. The rocks have a NE-SW strike direction and dip towards SE. This information was provided by the geologists and has been fundamental in the modelling process. Purple lines on Figure 8 indicate demarcations of lithological units as were mapped by the geologists (Nilsson et al.,2021).

The nickel prospect within a 195 m x 125 m cyan rectangle is our area of interest. Many rock samples (black dots) were collected from the survey area for petrophysical and geological analysis. Five (5) samples were identified as nickel ore and were found within the smaller cyan box.

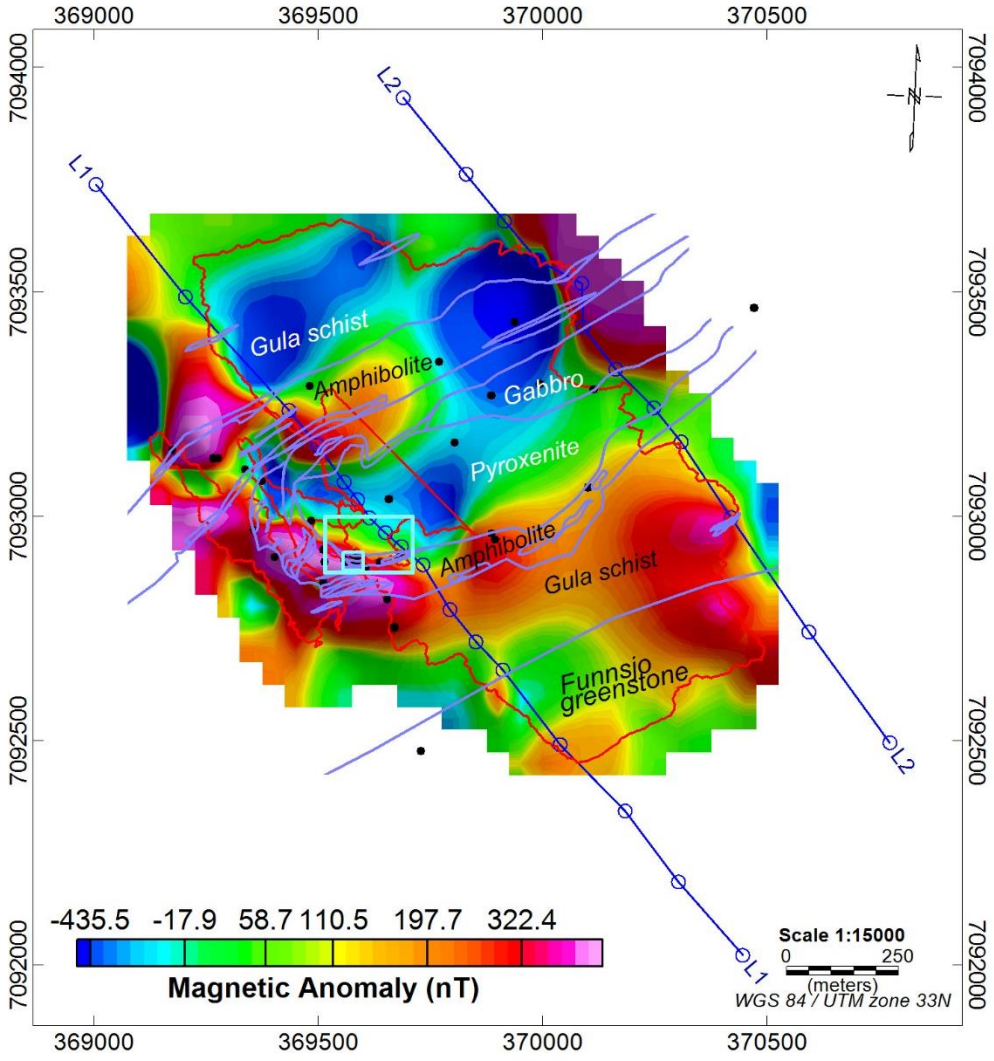

Figure 8: Location of the petrophysical and geological data in the survey area. The gravity profiles L1 and L2 are shown in blue. The boxes mark the prospect area. Purple lines demarcate lithological units (Nilsson et al.,2021).

Density and susceptibility measurements

Petrophysical data for density and magnetisation from 45 samples (Nilsson et al.,2021) collected from the survey area were available during this work. Mean values of density and susceptibility readings of each rock type are displayed in Table 1. The range of susceptibility values from pyroxenite and amphibolite rocks is quite wide to calculate a single mean value. Therefore, these rocks were divided into two groups. Susceptibility values higher than 0.002 SI were grouped as a high magnetic (_Hmg) group and provided its own mean value. Similarly, susceptibility values for the ore samples are very diverse and hence not averaged.

Table 1: Density and susceptibility mean values.

Lithology	Density (kg/m^3)	Susceptibility (SI)	M/I/D	colour code
Background	2670	0		
Amphibolite	3040	0.00132		
Amphibolite_Hmg	3040	0.00435	0.4/0/0	
BIF	3040	0.05970	1/0/0	
BIF_1	3040	0.00450		
Funnsjø greenstone	3025	0.00680		
Gabbro	2910	0.00085		
Gula schist	2790	0.00078		
Pyroxenite	3000	0.00123	0.5/0/0	
Pyroxenite_Hmg	3000	0.00467		
Pyroxenite_OF	2910	0.00200	0.5/0/0	
SKJ 20 - 34	3030	0.15750		ore
SKJ 20 - 36	3240	0.35050		ore
SKJ 20 - 37	3470	0.29420		ore
SKJ 20 - 38	3270	0.16570		ore
SKJ 20 - 42	4080	0.06370		ore

BIF = banded iron formation
Pyroxenite_OF = Olivine free pyroxenite.
M/I/D= Magnetic remanence (A/m), Inclination and Declination (degree).

Modelling results: L1 and L2

Gravity and ground magnetic data were used in 2D modelling of the two lines. Magnetic profiles are not along the gravity lines; therefore, the data was gridded (50 m x 50 m) and data points extracted along the two lines.

The geological map along line L1 suggested the presence of Gula group intruded by pyroxenite and bordering Funnsjø greenstone (Funnsjøgruppen) at the southwest (Wolf,1977). The 2D model (Figure 9) displays the same pattern.

The lithological pattern of L2 (Figure 10) is similar to that of L1. In addition, L2 crosses the gabbro intrusion which is not found in L1. The pyroxenite and gabbro intrusions are believed to represent two independent magma pulses (Nilsson et al.,2021).

On average, the intrusions (gabbro + pyroxenite) are about 215 – 260 m wide and 90 -270 m thick. Figure 9 and Figure 10 are model profiles down to 0 m (mean sea level) shown at vertical exaggeration (VE) of 1.26 and 1.0 respectively. Models extending to larger depth are shown in Figure 41 and Figure 42 in appendix A2.

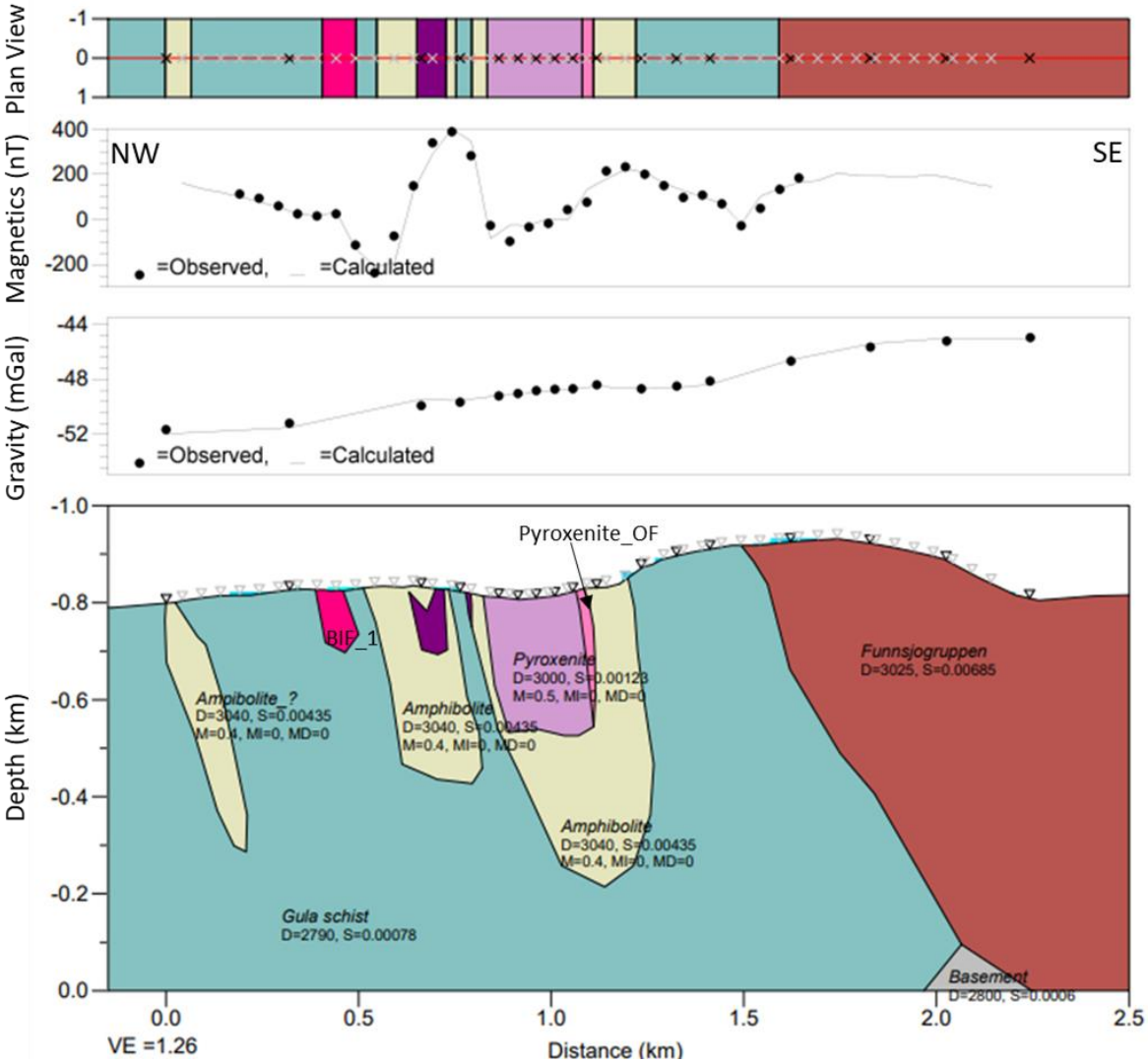

Figure 9: A 2D profile along the western line L1. Triangles on the surface are locations of gravity stations (black) and magnetic data points (grey). The gravity and magnetic profiles in the middle show the calculated data (solid lines) fitting the observed data (dots). The plan view is taken at (-)750 m above msl.

The pyroxenite intrusion in L1 is about 260 m wide and 270 m thick.

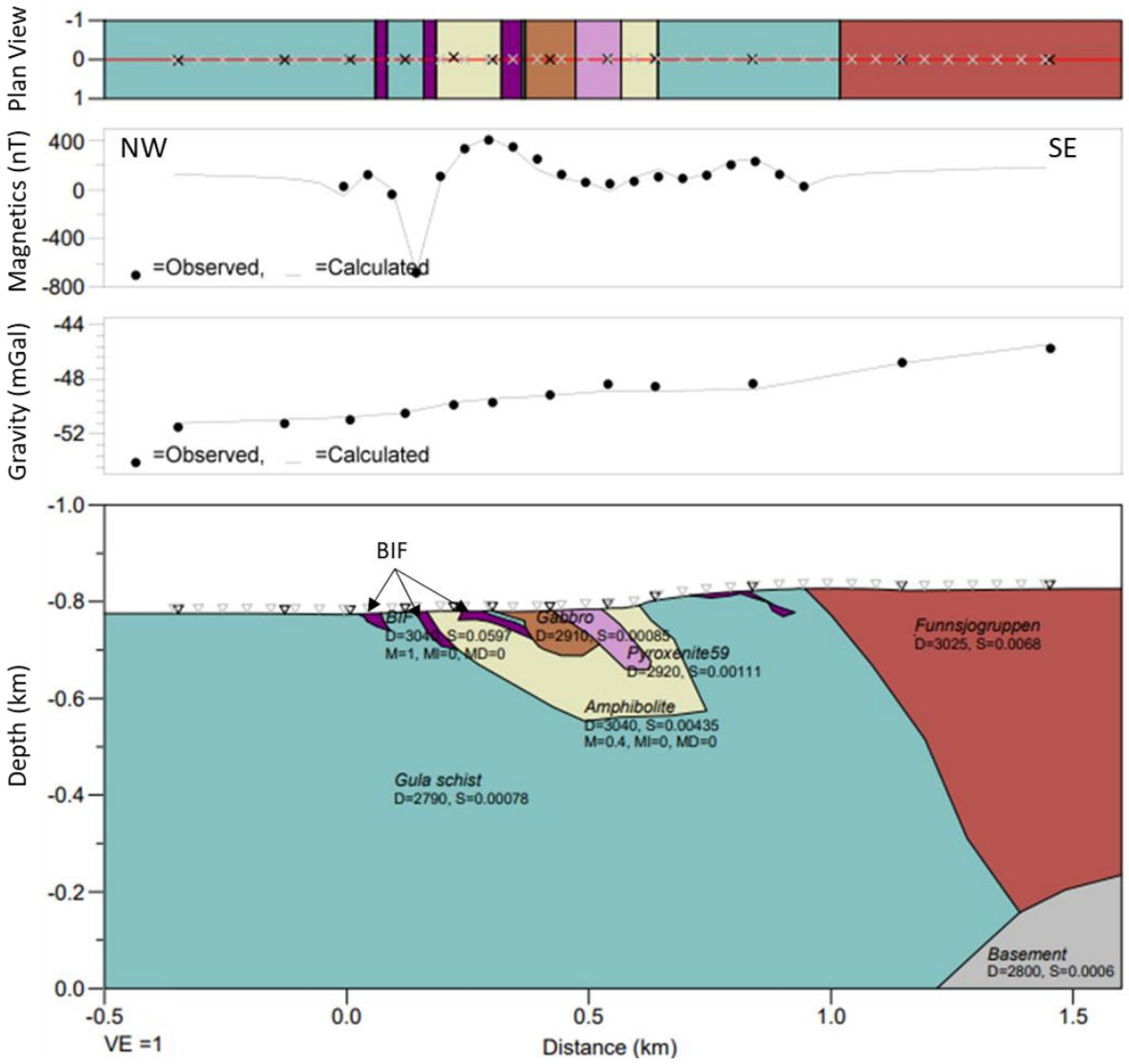

Figure 10: A 2D profile along the eastern line L2. Triangles on the surface are locations of gravity stations (black) and magnetic data points (grey). The gravity and magnetic profiles in the middle show the calculated data (solid lines) fitting the observed data (dots). The plan view is taken at (-)750 m above msl.

The pyroxenite intrusion in L2 is about 100 m wide and 120 m thick. The gabbro intrusion is about 115 m wide and 90 m thick. There is no petrophysical samples between the amphibolite and the Funnsjo greenstone. The observed high magnetic anomaly at this location is fitted by a high magnetic BIF (0.05970 SI).

5. VOXI 3D INVERSION OF MAGNETIC DATA

As part of data interpretation, a 3D inversion was conducted using VOXI software which is a Geosoft plugin (Oasis Montaj 9.8.1). A VOXI 3D susceptibility inversion inverts magnetic data to produce 3D voxels of magnetic susceptibility. This inversion method assumes the rock susceptibility is due to weak induced magnetization (Li, Y., 2016). To get a better understanding of how VOXI works and what to expect, the inversion was initially performed on a synthetic data.

The 3D inversion was not carried out on gravity data due to the nature of the survey configuration. The two lines are far apart for 3D representation of the prospect which is our area of interest.

5.1 VOXI 3D inversion of synthetic data

For synthetic data, a simple geo-model (Figure 12) was built using GM-SYS 3D plugin in Geosoft (Oasis Montaj 9.8.1) and 3D forward modelling was performed to produce the data. The model is comprised of a high magnetic body (target) with magnetic susceptibility and density of 0.05 SI and 3040 kg/m^3, respectively. Surrounding the target is a low magnetic rock with magnetic susceptibility and density of 0.00078 SI and 2790 kg/m^3, respectively. The target and the host replicate the amphibolite and BIF in the central part of the survey area which is surrounded by Gula schist (host). The topography used is a digital elevation map for Brattbakken survey area.

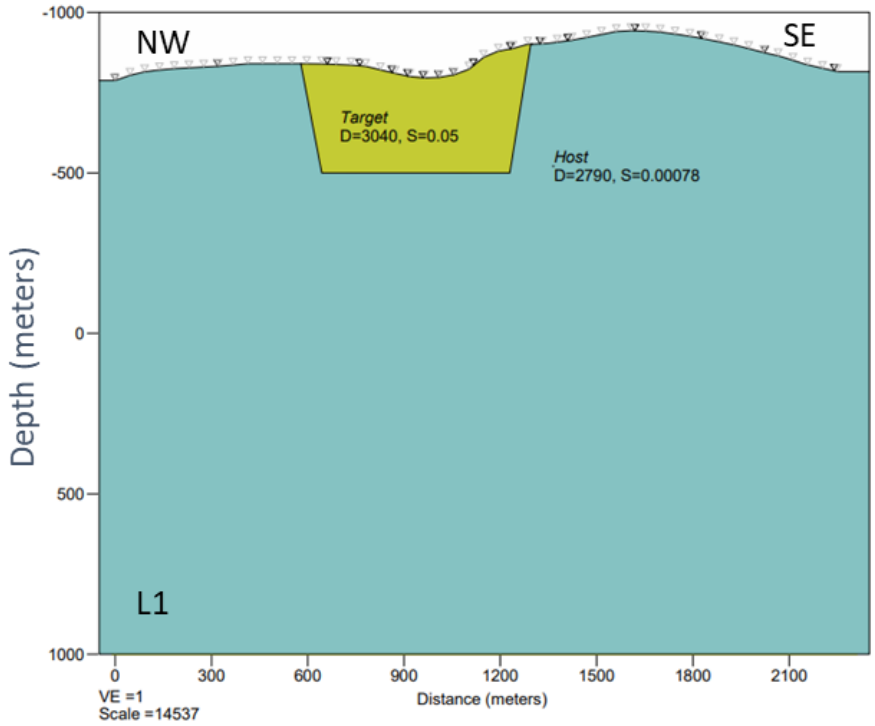

Figure 11: A 2D section of the synthetic model along line L1. Triangles on the surface of the model are locations of gravity stations (black) and magnetic data points (grey).

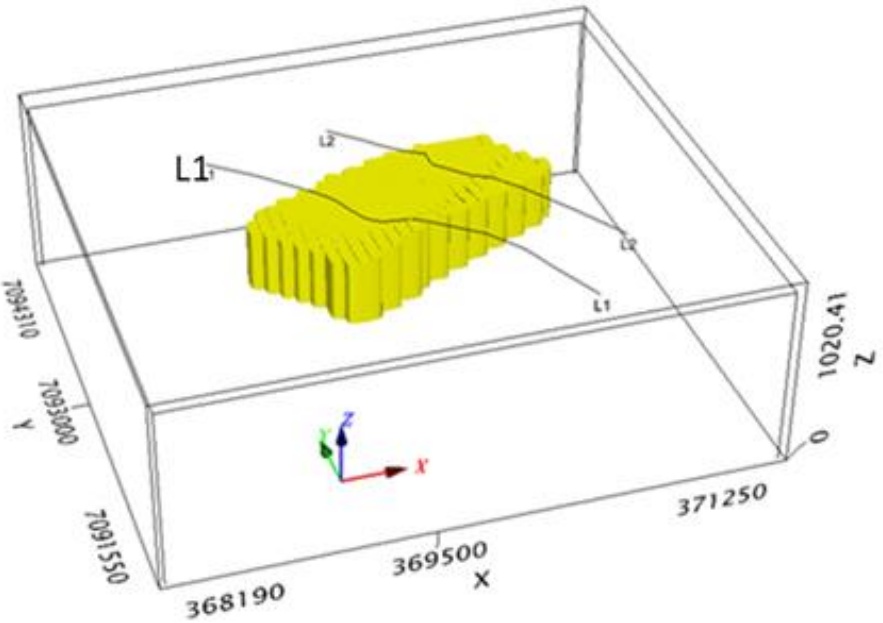

Figure 12: A 3D view of the model showing the target, susceptibility >0.005 SI.

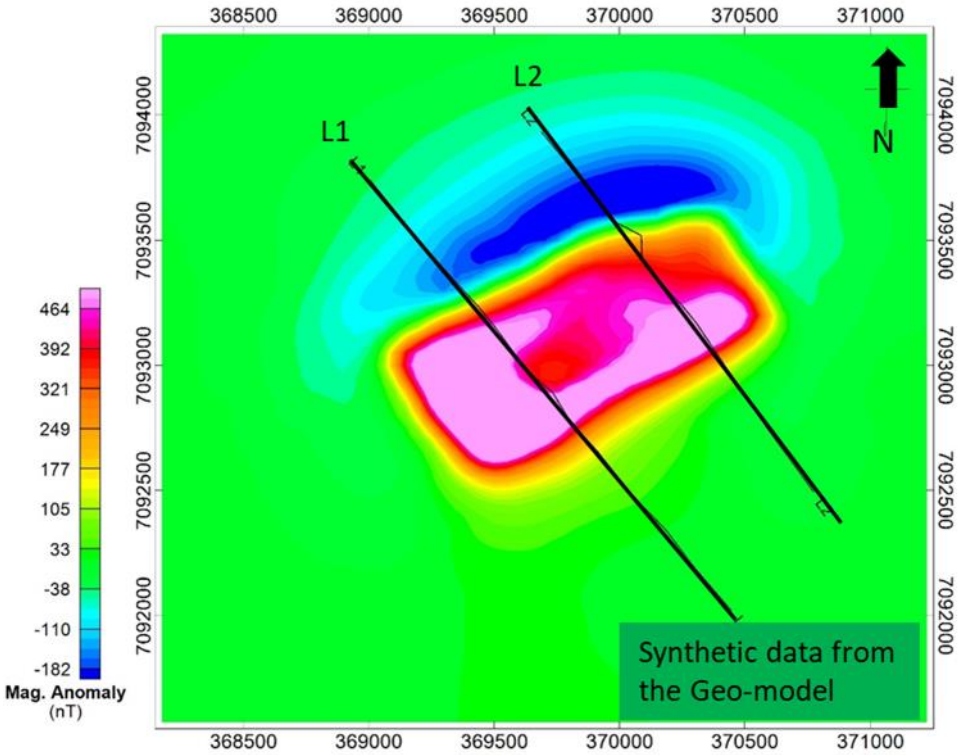

Figure 13: Synthetic data from the 3D geo-model. Black lines are location of gravity profiles L1 and L2.

The inversion was first run unconstrained, that is, only data driven. Unconstrained inversion has a large window of freedom in updating the model; spatially and with susceptibility range without being strongly penalized. The inversion was run with default parameters (refer the VOXI inversion menu). In the absence of reference models, the guiding parameter is the data misfit. The inversion will iteratively update the starting model to produce data which is as close as possible to the observed data within the uncertainty range. The inversion will stop when the target misfit is reached.

Targeted misfit reduced Chi-square (RCS) of 1 (default) was used. The RCS (χ^2_{red}) is defined by Equation 5-1 below.

$$\chi^2 red = \frac{\chi^2}{\nu} = \frac{1}{\nu}\sum\frac{(O-E)^2}{\sigma^2} \qquad 5\text{-}1$$

where: O is observed data, E is calculated/predicted data, v is number of data points and σ is a fit error or generalized standard deviation of the measurement (that is, includes data uncertainty).

An inversion was set with cell sizes of 65 m x 65 m x 10 m for x, y, z at the area of interest and cell size in z direction was set to gradually increase (1%) with depth as data sensitivity decreases. Model depth is 4000 m. The inversion was run with linear background removal to enhance localized anomalies. The background removal reduces effects of regional structures like basements which extend beyond the model domain.

The inversion result is shown in Figure 14 and Figure 15. Unconstrained inversion produced significant artefacts. At the central area where the topography is lower, the target is imaged deeper. As a result, magnetic susceptibility at the shallow section is lower than the surrounding. However, the vertical contacts of the target are resolved reasonably well. The model converged to RCS of 1 at iteration 3.

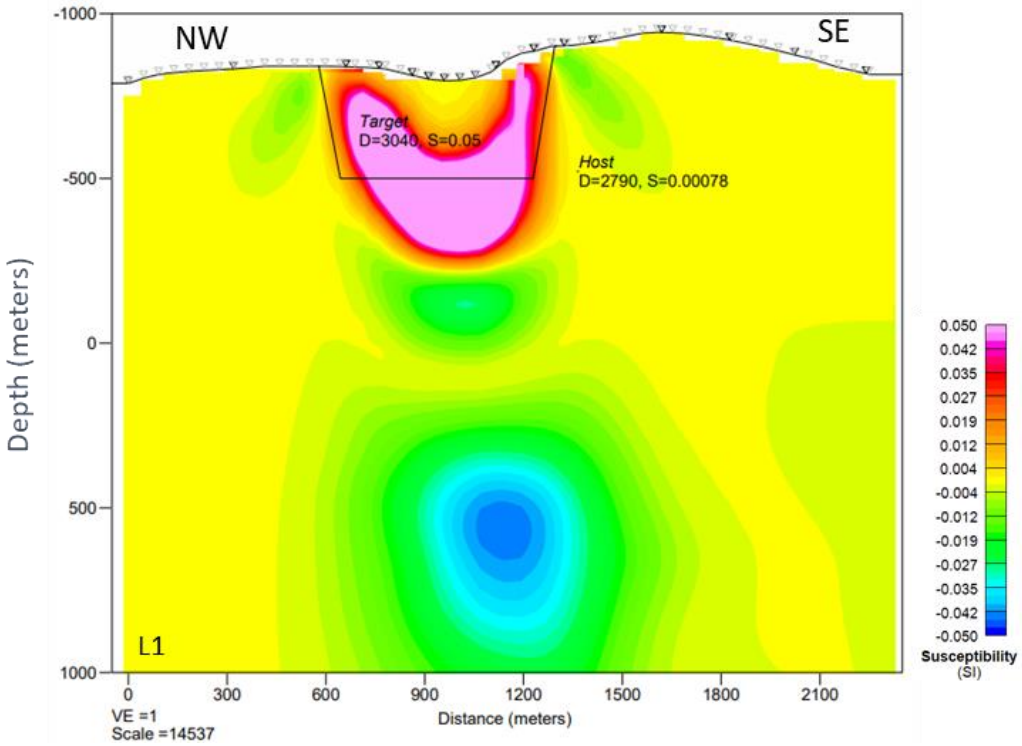

Figure 14: Unconstrained inversion results of synthetic data shown along line L1. Triangles on the surface are locations of gravity stations (black) and magnetic data points (grey).

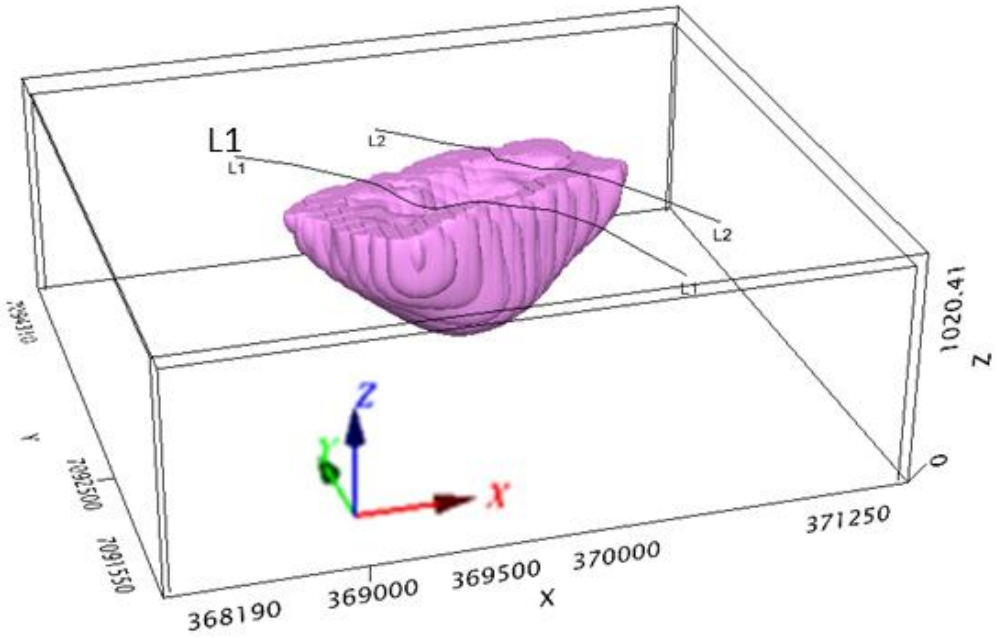

Figure 15: Unconstrained inversion result of the synthetic data showing the recovered target and location of line L1.

To mitigate the artefacts, lower (Lb) and upper (Ub) susceptibility boundaries were applied to softly constrain the inversion. Lb and Ub of 0 and 1 respectively improved the results and 0.0005 and 0.06 respectively gave the best result (Figure 16). The lower and upper bound values are based on the knowledge derived from petrophysical data.

The constrained inversion (Figure 16) has remarkably resolved the target's vertical and horizonal position (c) as well as the susceptibility values (a).

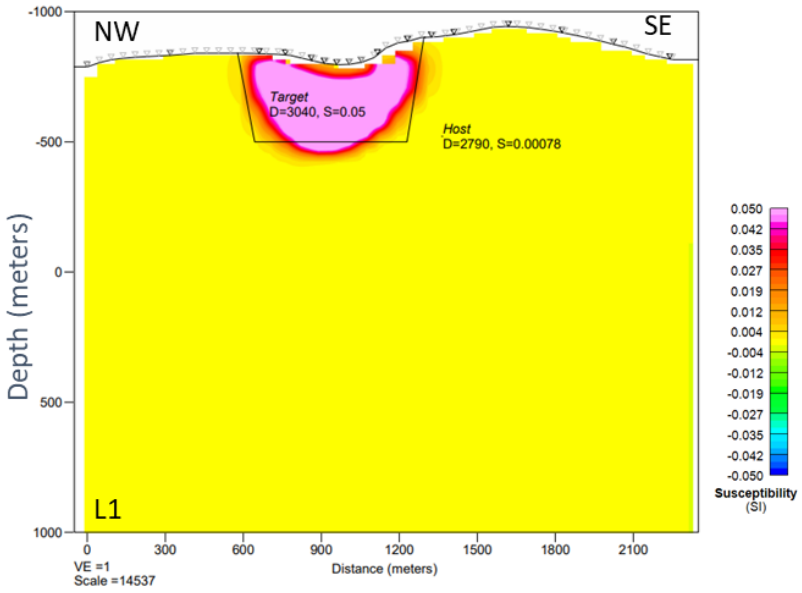

(a) A 2D section at line L1. The black outline is a true model target.

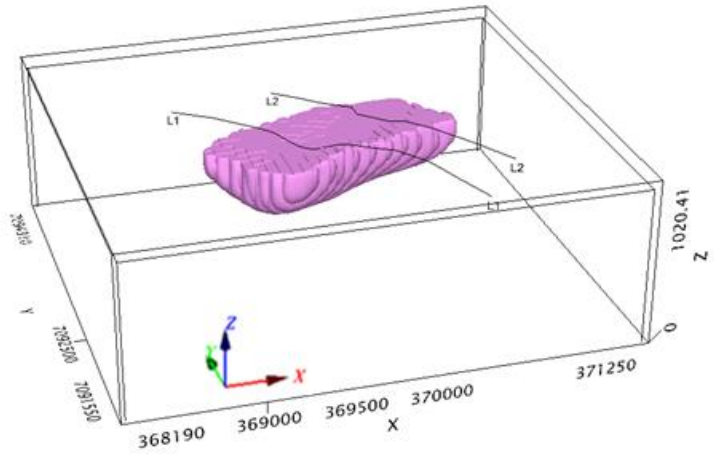

(b) 3D view of the model showing the recovered target and location of line L1.

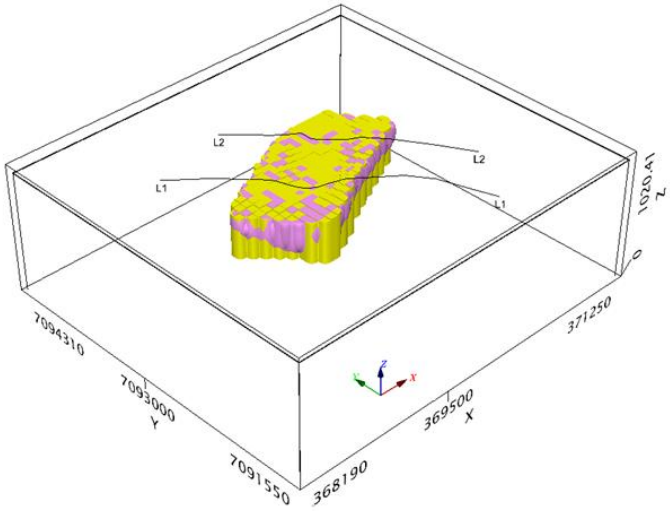

(c) Inversion recovered target (pink) superimposed on the target from the true model (yellow).

Figure 16: Constrained inversion result. The target is well recovered.

Data misfit

The success of inversion is measured by the geological soundness of the produced models and how mathematically, the resulting data fits the input (observed) data. The reduced chi square (RCS) misfit shown in Figure 17 is a function of a weighted difference between the observed and the calculated data (*Equation 5-1*)). Hence:

- RCS =1: a good data fit. The data difference is within the predefined fit error (uncertainty).
- RCS < 1 means the model is overfitting the data or the uncertainty is overestimated.
- RCS > 1 means poor data fit or the uncertainty is underestimated.

For this inversion, the fit error was set to absolute value of 2 nT and start model of 0.0 SI. The absolute error is useful in scenarios where we want to minimize the effects of weak response or noise. Data will preferentially fit strong anomalies. The absolute error is a good choice for this data because our anomaly is large and we want to recover it precisely. The inversion has on average fitted the data within the defined fit error. The inversion started at RCS error of 6500 and converged to RCS = 1 at iteration 2 and stopped at iteration 3. The calculated data from the inversion result (Figure 18) fits the observed data (Figure 13).

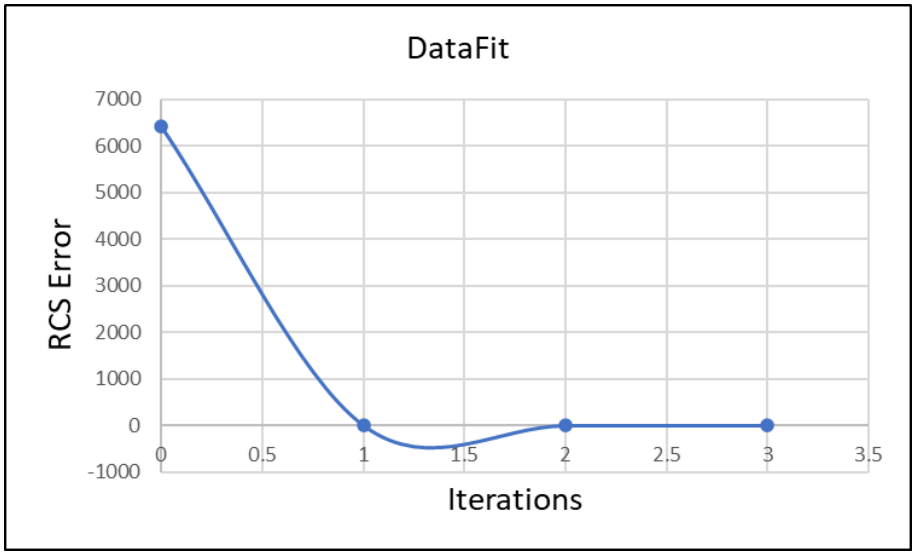

Figure 17: Convergence curve of the synthetic data inversion.

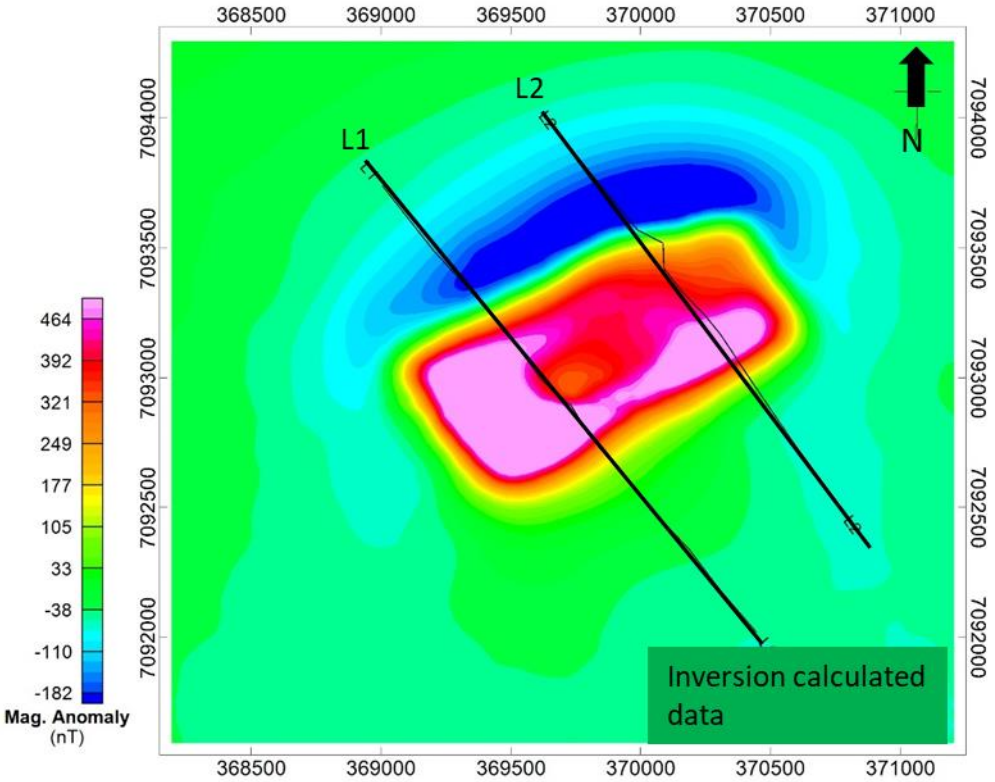

Figure 18: Calculated data from the inversion result. Black lines are location of gravity profiles L1 and L2.

5.2 VOXI 3D inversion of real data

The inversion was performed with linear background removal to enhance localized anomalies. An inversion mesh of 4000 m deep was set with cell sizes of 65 m x 65 m x 10 m for x, y, z at the area of interest and cell size in z direction was set to gradually increase with depth (by 1%) as data sensitivity decreases. As observed in the synthetic tests, upper and lower bound have significant impact on the results. On real data, lower bound was set to 0.0005 SI and upper bound 0.3 SI. For a better 3D coverage, Snåsa airborne data (Figure 19) was used as input to this inversion.

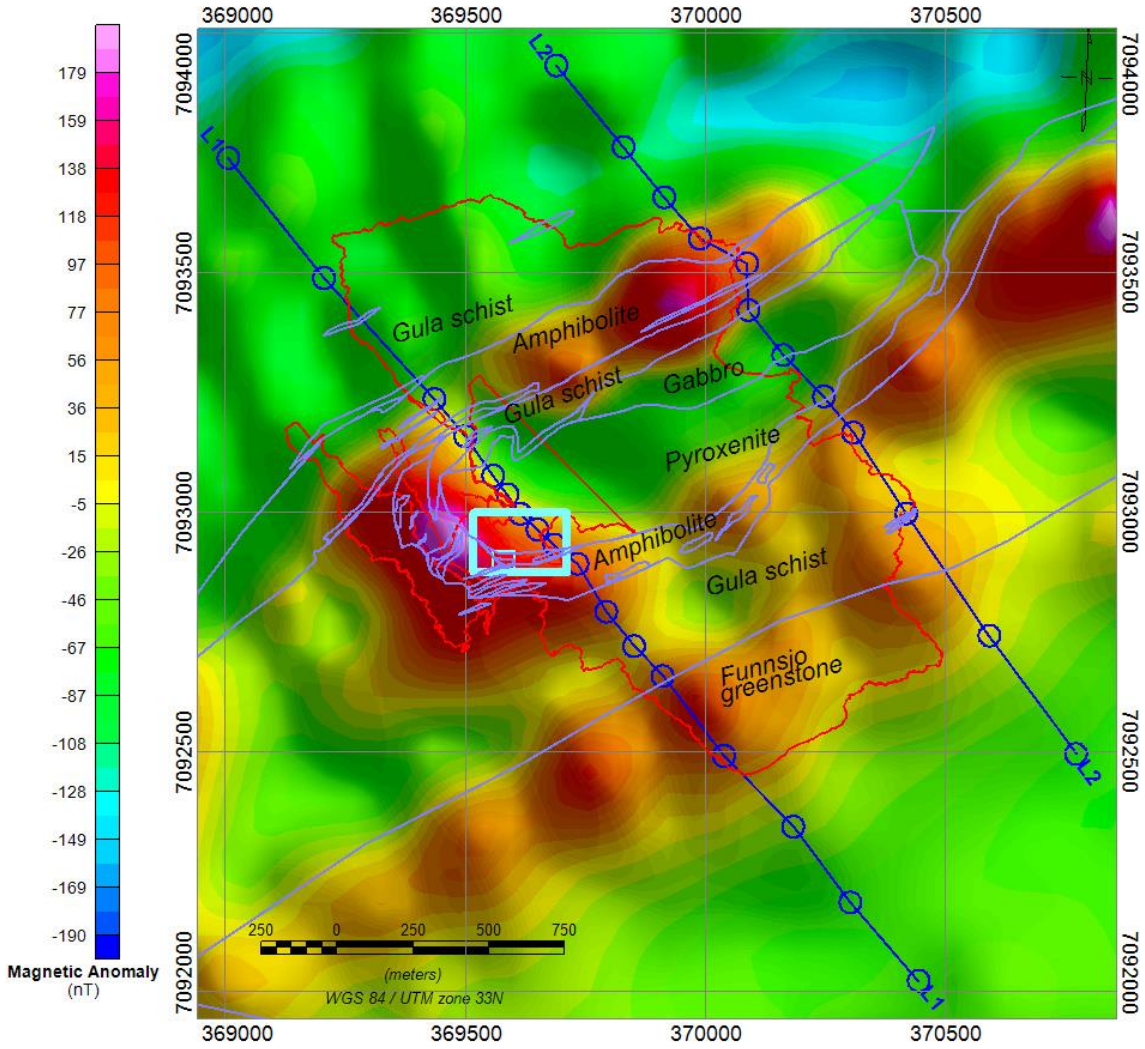

Figure 19. Snåsa airborne data acquired in year 2020. The gravity profiles L1 and L2 are shown in blue. The box marks the prospect area. Helicopter flight lines are in cyan and purple lines demarcate lithological units.

WNE-ESW lines in Figure 19 are magnetic flight lines at 200 m apart. The nickel prospect area is highlighted by a cyan coloured rectangle. Purple lines are lithological demarcations as mapped by the geologists (Nilsson et al.,2021).

Positive anomalies are observed at Funnsjø greenstone and at the Gula group especially within the amphibolite. The observations are consistent with petrophysical samples as shown in Table 1 where the amphibolite records high susceptibility values. Also, positive anomalies within the Gula group are caused by BIF.

3D inversion results are shown in Figure 20 to Figure 23.

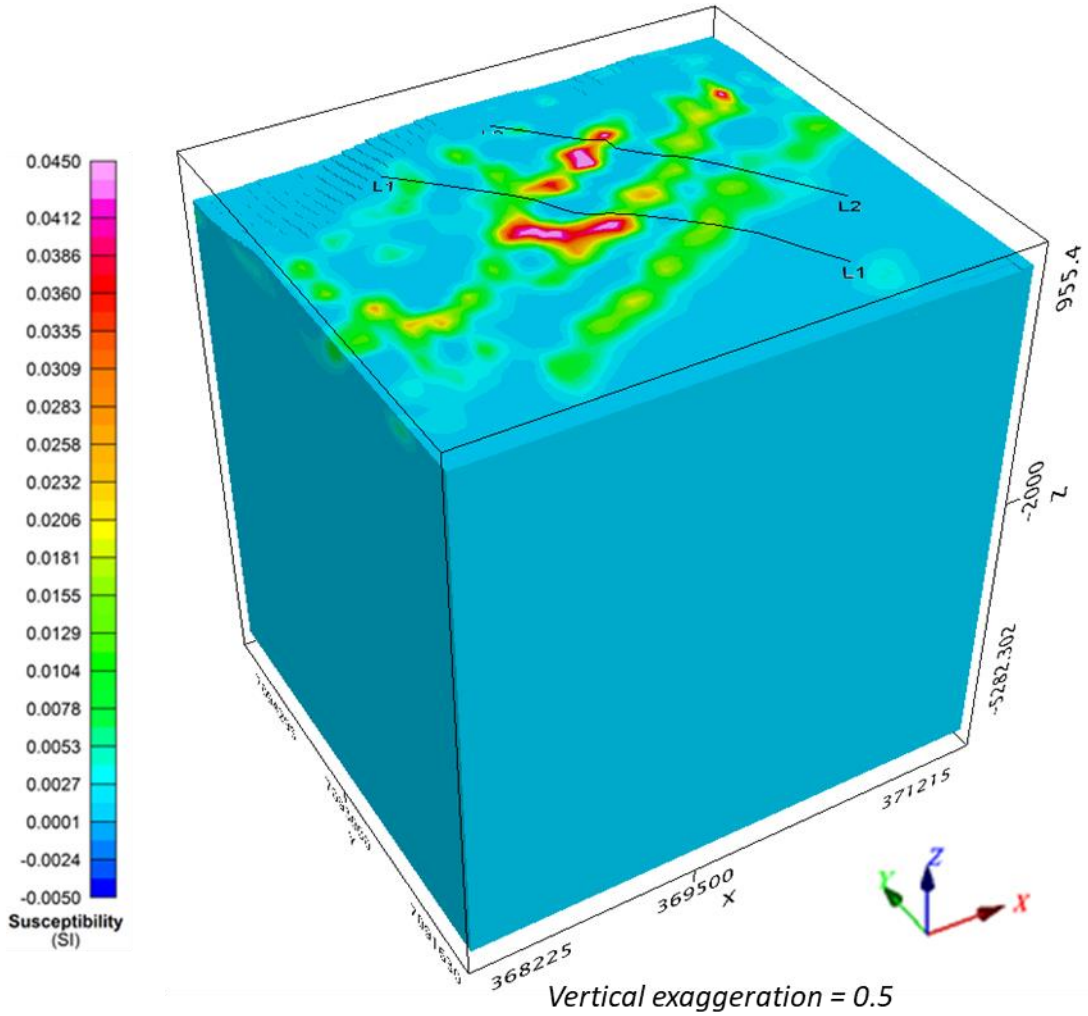

Figure 20: A 3D cube of inversion result of airborne data showing susceptibility distribution in x, y, z. Black lines are locations of gravity profiles L1 and L2.

Figure 21 shows the inverted model at selected susceptibility ranges to highlight anomalies and their link to geological units. Strong anomalies labelled A and B in this figure are most likely caused by BIF. The nickel ore is blended in anomaly A.

Figure 21 (a): map view at susceptibility greater than 0.00435 SI. This cut-off value represents a mean value for high magnetic amphibolite (Table 1). This figure indicates a lateral distribution of amphibolite and other high susceptibility rocks including the Funnsjø greenstone towards the southeast. Figure 21 (b) shows the lateral and vertical susceptibility distribution along lines L1, L2 and an arbitrary line crossing L1 and L2.

Generally, the inversion result has well reproduced the input/observed data (Figure 19).

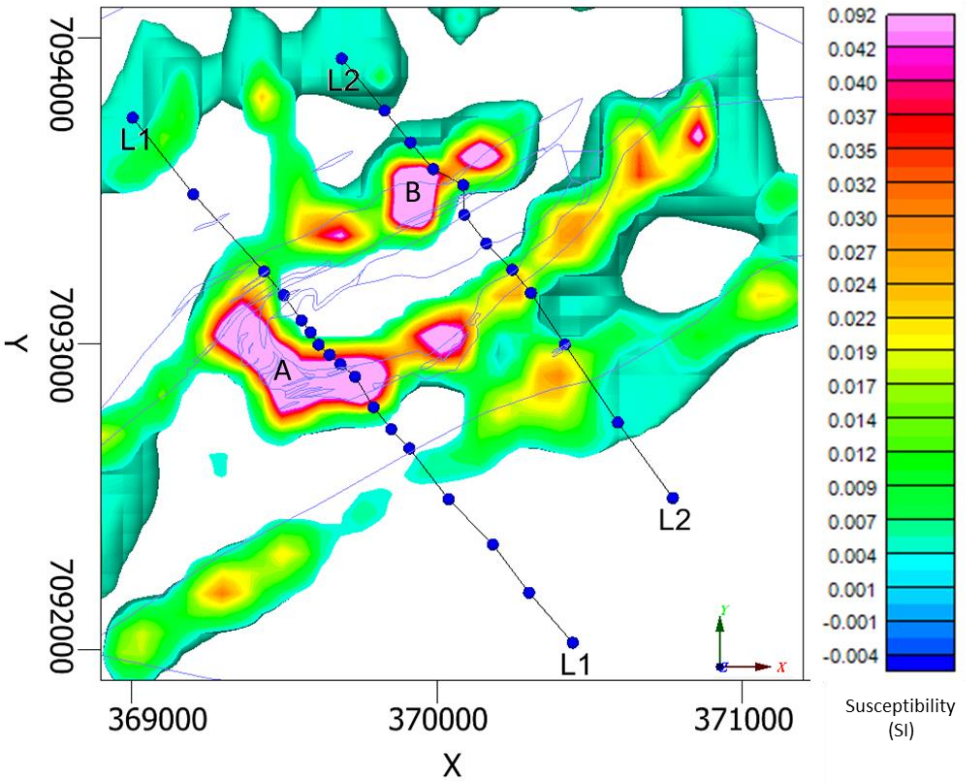

(a) Map view at 670 m above msl. Susceptibility > 0.00435 SI, the average value of the high magnetic amphibolite. Strong magnetic anomalies A and B extend to lines L1 and L2, respectively.

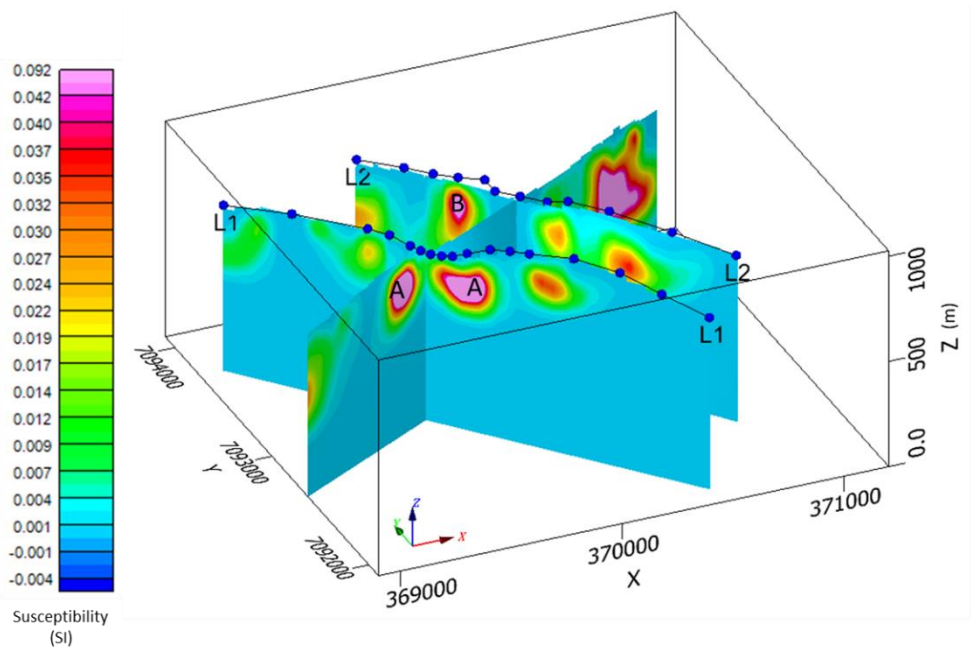

(b) 3D view along profiles L1, L2 and an arbitrary crossing line.

Figure 21: 3D inverted model showing a spatial distribution of magnetic anomalies. The gravity profiles L1 and L2 are shown in blue and geological boundaries in purple lines for reference.

The cross-sections on Figure 22 and Figure 23 show susceptibility distribution horizontally and with depth. Superimposed on the sections (black outlines) are the 2D modelling results for comparison. Generally, the anomalies fit the 2D modelling results except that the amphibolite (0.00435 SI) underlaying pyroxenite was modelled too thick on L1, or 3D inversion modelled it thinner. Inversion result without background removal (Figure 22 b) gives the same result concerning the amphibolite. To verify the thickness of the amphibolite unit below the pyroxene, 2D models were revisited (Figure 24 to Figure 26).

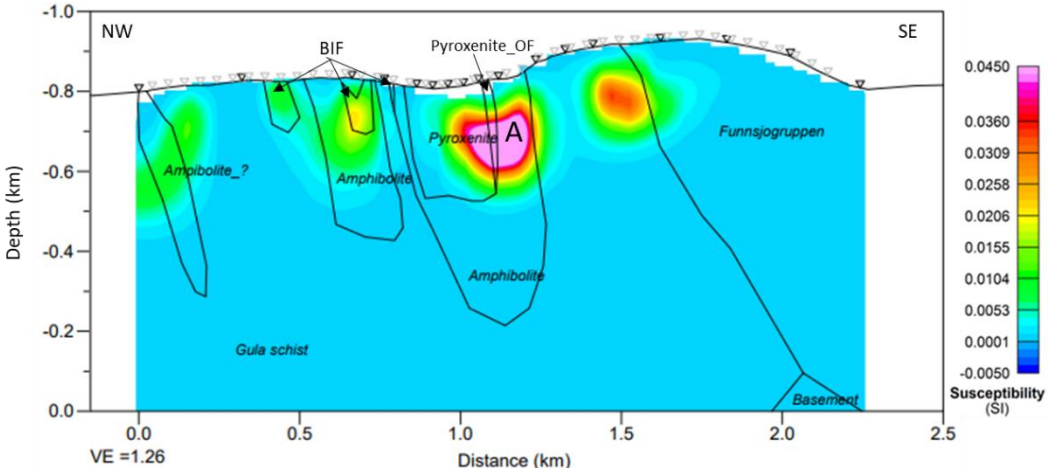

(a) Line L1: 3D inversion with linear background removal.

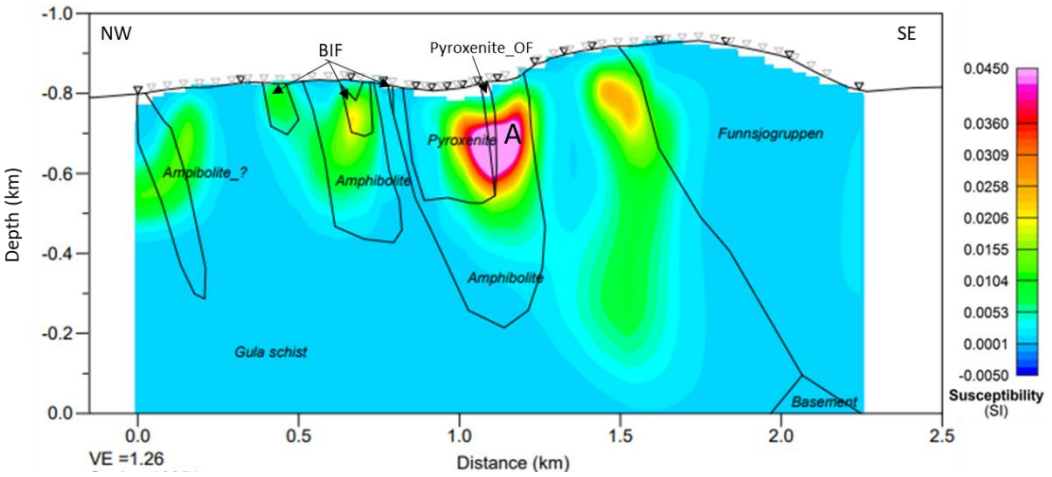

(b) Line L1: 3D inversion without background removal.

Figure 22: 3D inversion results showing vertical sections along line L1. Superimposed on the sections (black outlines) are the 2D modelling results for comparison.

BIF units of considerable size as modelled in 2D are also recovered in the 3D models. A strong anomaly A which extends towards line L1 is coinciding with olivine free pyroxenite, a host of the nickel ore.

Figure 23 displays 3D inversion result along line L2. Anomaly B fits the modelled BIF in the area. There is a deep-seated anomaly towards southeast near the Funnsjo greenstone. This anomaly does not match the assumed BIF on the surface. Also, the amphibolite on 2D modelling is relatively thin compared to the 3D inversion result.

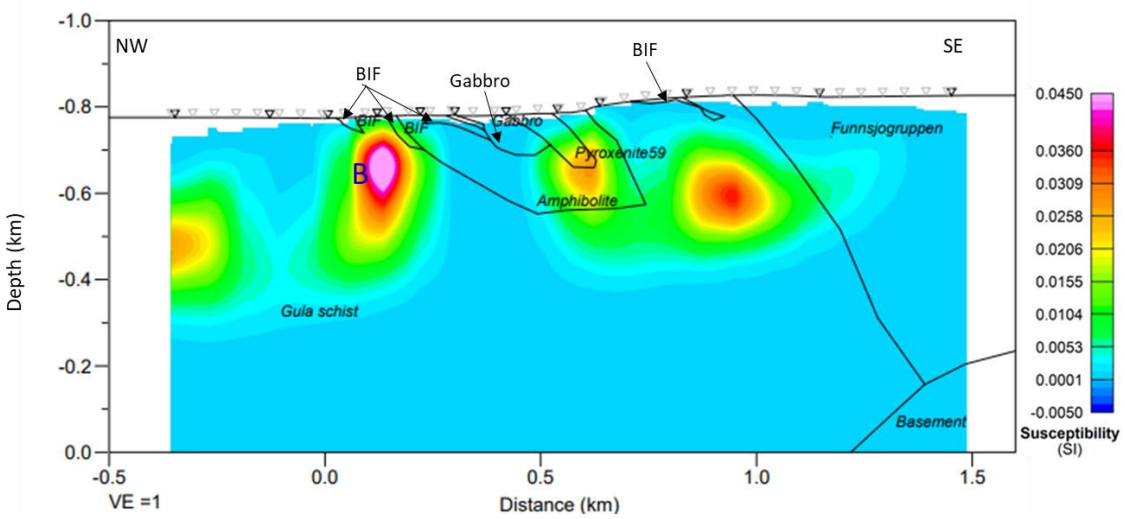

Figure 23: A vertical section along line L2 from inversion with linear background removal. Superimposed on the section (black outlines) is the 2D modelling results for comparison.

5.3 Revised 2D models based on 3D inversion results.

The amphibolite thickness in 2D models was changed to fit the anomalies in the 3D model. Amphibolite thickness on L1 (Figure 25) is reduced from 600 m to 386 m while on L2 (Figure 26) is increased from 220 m to 408 m. The new amphibolite thicknesses on L1 and L2 are more similar than in the old models. The new models fit the gravity and magnetic curves equally well.

The revised 2D model on L1 includes anomaly A. The anomaly is fitted with density D = 3000 kg/m^3 and susceptibility S = 0.02 SI. Introduction of Anomaly A fits better the high magnetic value on the curve which was otherwise fitted by increased amphibolite thickness. Susceptibility values for the rest of the rock units are as given in Table 1.

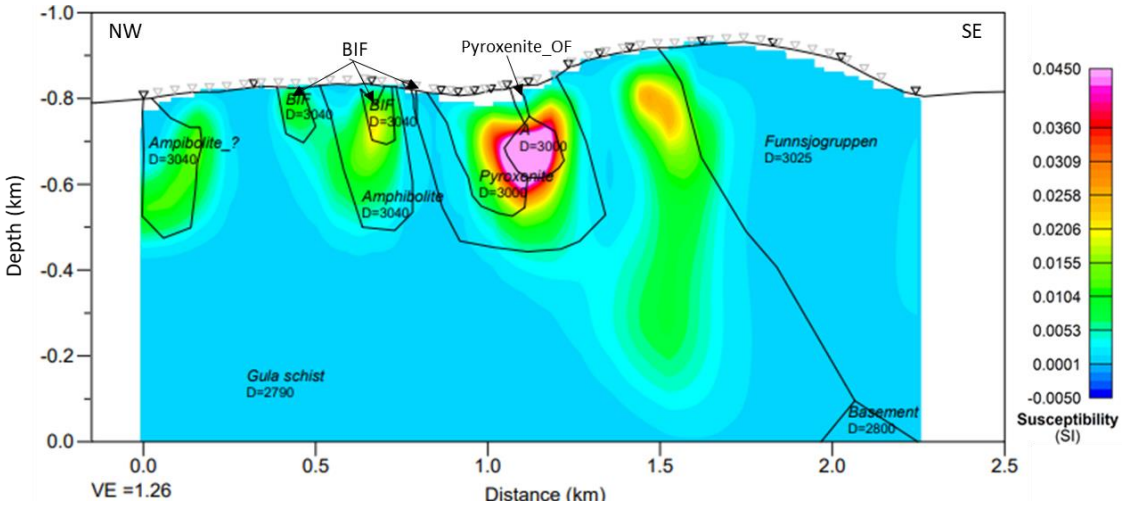

Figure 24: A revised 2D model (black outlines) along line L1 fitting the VOXI 3D inverted model.

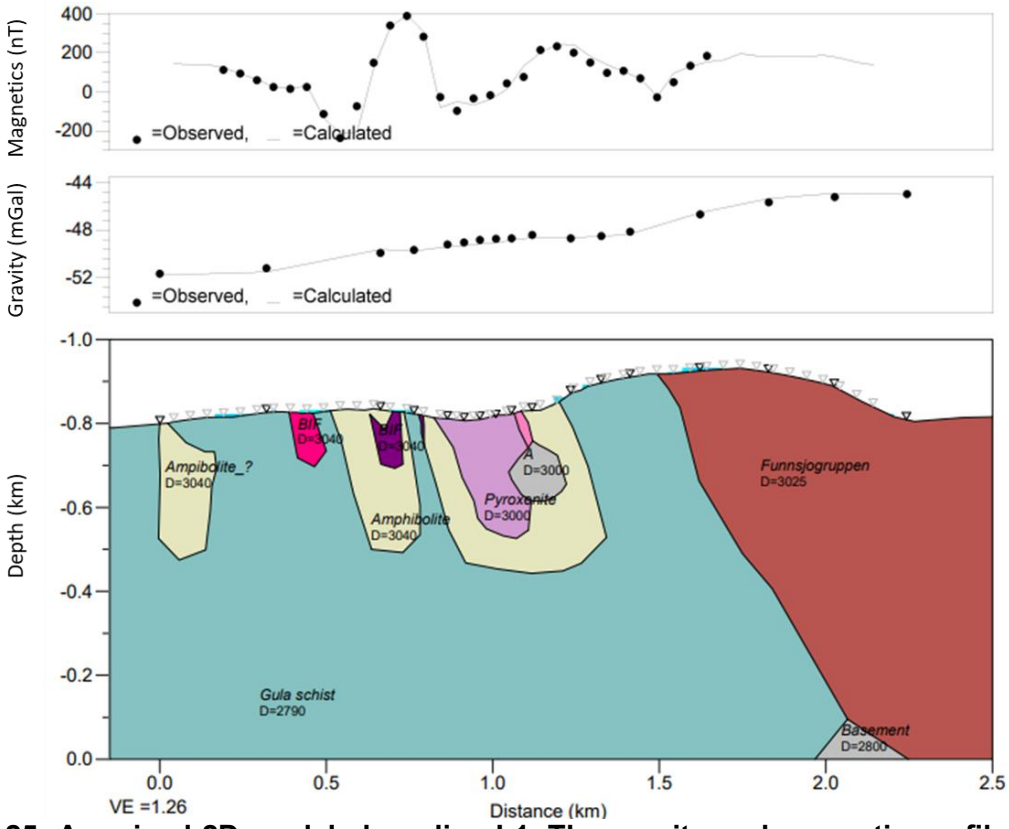

Figure 25: A revised 2D model along line L1. The gravity and magnetic profiles show the calculated data (solid lines) fitting the observed data (dots).

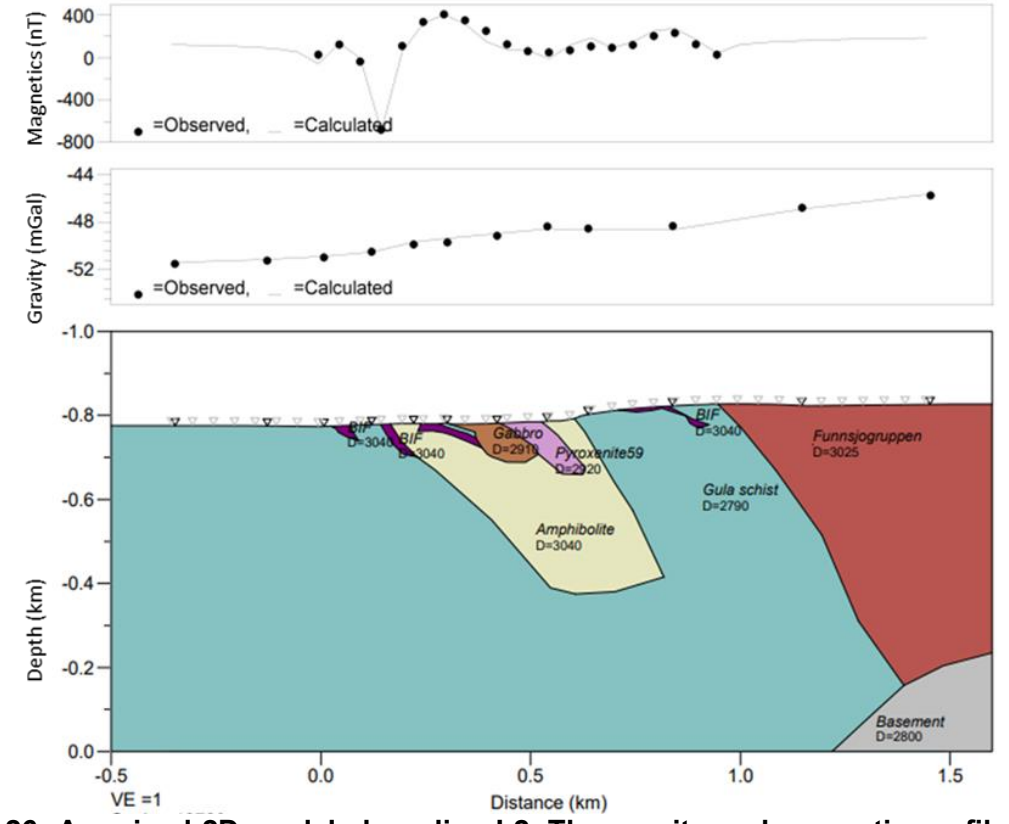

Figure 26: A revised 2D model along line L2. The gravity and magnetic profiles show the calculated data (solid lines) fitting the observed data (dots).

3D inversion - Data misfit

The fit error (uncertainty value) was set to absolute value of 2.77 nT (which is 5% of the standard deviation of the data). The inversion has on average fitted the data within the uncertainty range. The inversion started at RCS error of 400 and converged to RCS = 1 at iteration 2 and stopped at iteration 3.

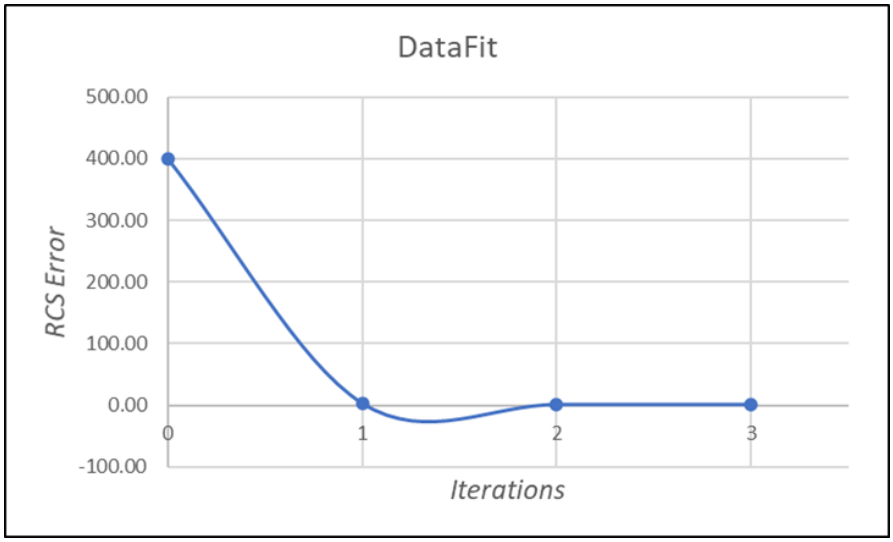

Figure 27: Convergence curve of the real data inversion.

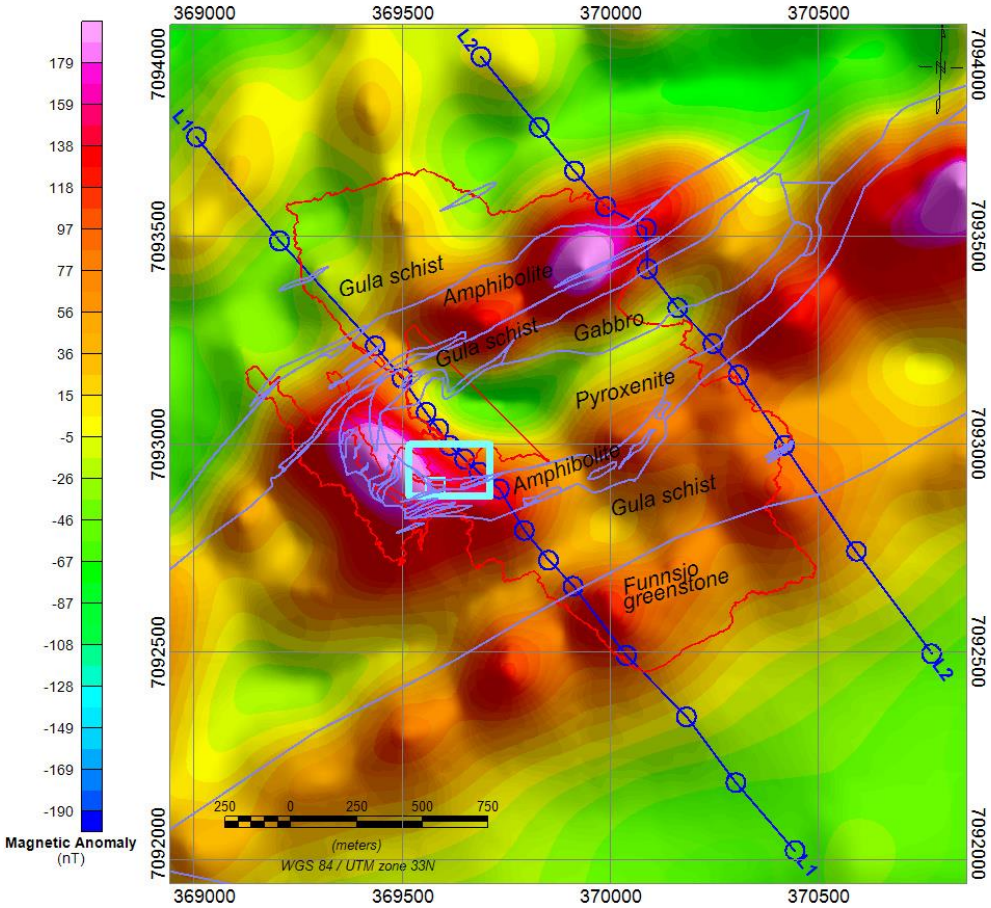

Figure 28: Calculated data from the inversion result. This data fits the observed data (Figure 19). The gravity profiles L1 and L2 are shown in blue. The box marks the prospect area. Helicopter flight lines are in cyan and purple lines are lithological demarcations.

5.4 VOXI 3D inversion of the nickel prospect area

The input/observed ground magnetic data used in the inversion is shown in Figure 29. The inset image is 50 m x 50 m grid showing the location of the nickel ore prospect in the survey area. The prospect is within a 195 m x 125 m area (cyan rectangle). The ground magnetic data is used for this inversion because of good data coverage at the prospect area. However, the prospect is relatively small and hence re-griding into cell size of 5 m x 5 m was necessary to distinguish anomalies from the high magnetic background. The same cell size was used in the inversion.

Anomalies A to F are observed in the data. Dark red (random) lines are magnetic profiles. Green dots are locations of nickel ore samples and black dots are of other rock samples. The identified ore samples are found in the olivine-free (OF) pyroxenite rock. Pyroxenite samples P1 (0.0005 SI) reads the lowest susceptibility in the area and P2 at anomaly F, reads 0.0009 SI. Gula gabbro sample G1 (0.0042 SI) represent the highest susceptibility value of the side rocks in the vicinity. The blue circles are gravity stations in a segment of line L1. A very high susceptibility body at the bottom-left corner is excluded in the inversion.

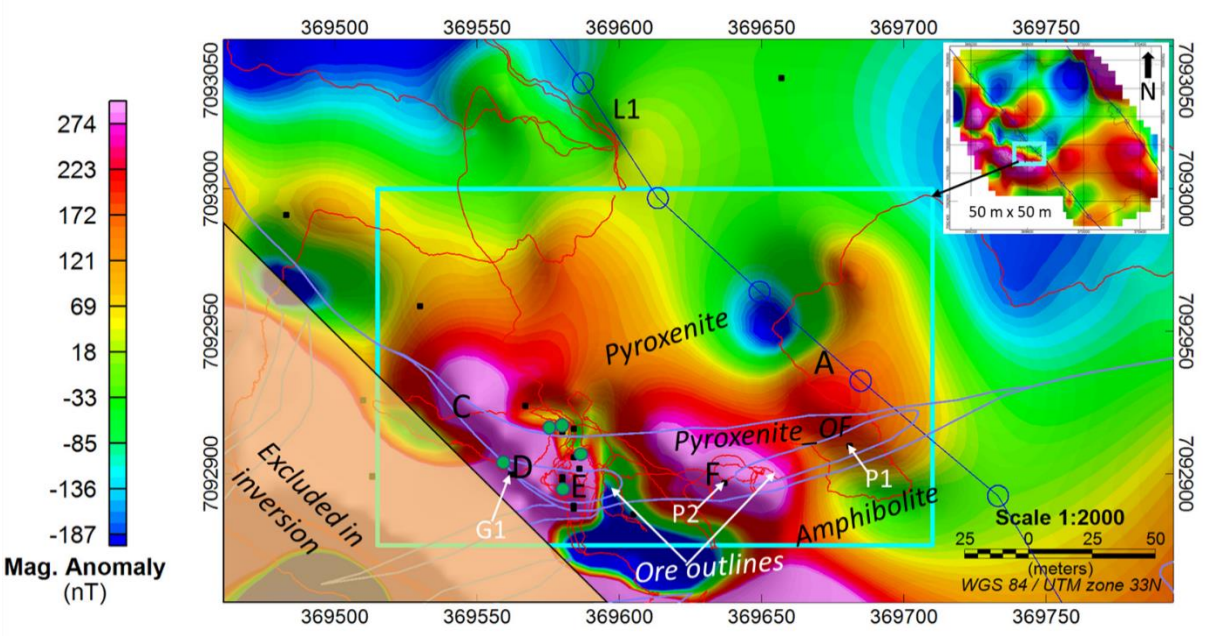

Figure 29: Measured data (5 m x 5 m grid) at nickel prospect area (Cyan box). The inset image shows the location of the prospect in the survey area. The gravity profile L1 is shown in blue and ground magnetic profiles in red. Geological boundaries are shown in purple.

The inverted area is 300 m x 170 m and 350 m deep. The inversion was set to run with lower and upper bounds of 0.0005 SI and 0.3 SI, respectively. Fit error of absolute value of 6.282 nT was used. The value is by default, 5% of the standard deviation of all data. A linear background removal on the data was applied.

Inversion results are shown in Figure 30 to Figure 36. The inversion converged to RCS of 1 at a second iteration. Anomalies A to F as identified in the observed data are recovered by the inversion.

Figure 30 (a) displays a 3D view of the inverted model across arbitrary lines showing susceptibility distribution in the cube. Figure 30 (b) shows a 3D view of the model at susceptibility > 0.0060 SI. This value is above the average high magnetic amphibolite and pyroxenite samples (Table 1). The entire cube is characterised by relatively high susceptibility values which is consistent with inversion result in Figure 21.

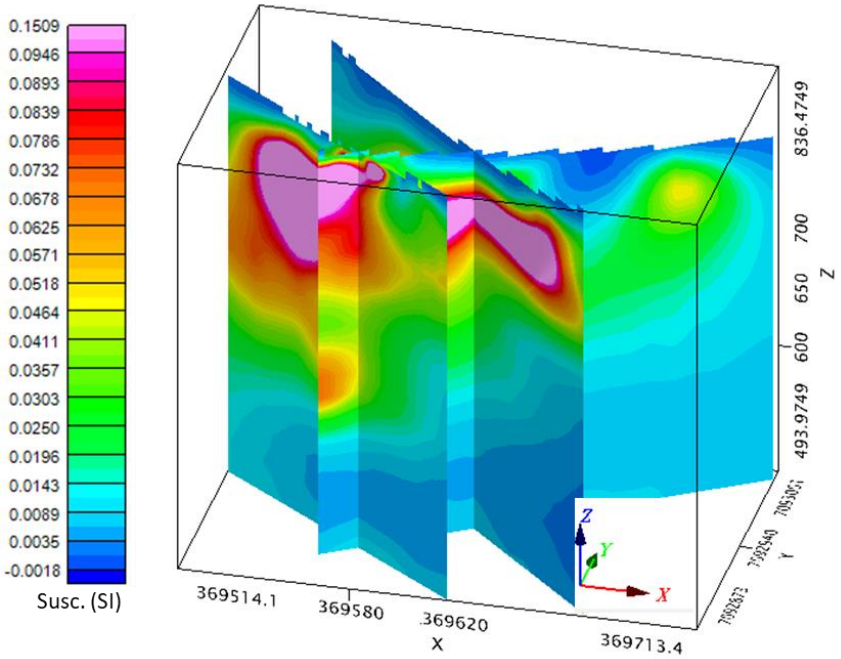

(a) 3D view of the inverted model across arbitrary lines.

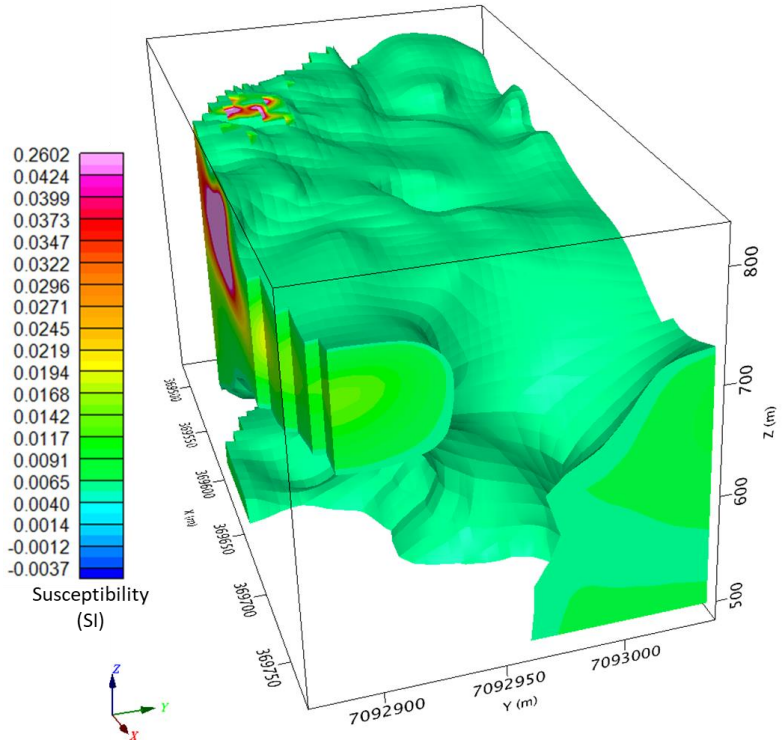

(b) 3D view of the inverted model at susceptibility cut-off > 0.006 SI. This value is higher than the average high magnetic none-ore samples.

Figure 30: 3D inversion result of the prospect area. Vertical exaggeration = 1.

Figure 31 shows the inversion calculated data (b) in comparison to the observed (a) data. In general, the inversion has produced a susceptibility model with calculated response replicating the observed data.

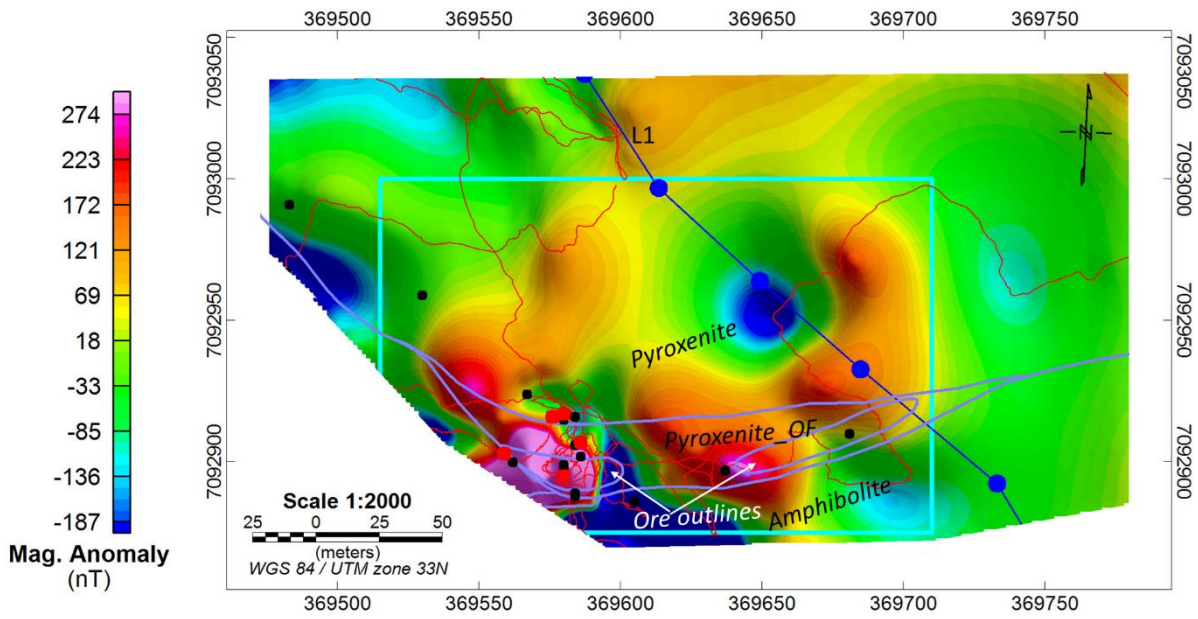

(a) Background removed observed data.

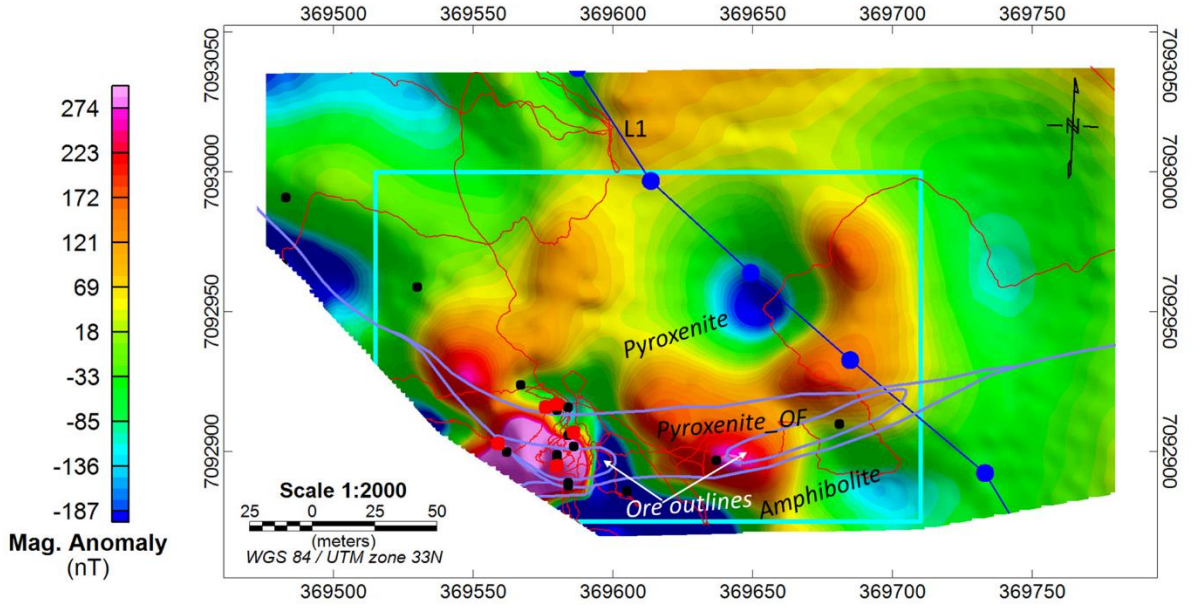

(b) Inversion calculated data.

Figure 31: Observed (a) and calculated (b) data from the inversion result. The box marks the prospect area. The gravity profiles L1 is shown in blue and ground magnetic profiles in red. Geological boundaries are in purple.

6. DATA INTERPRETATION AT THE PROSPECT AREA

The inversion result in Figure 32 and Figure 33 are shown at selected susceptibility range to emphasize on the recovered anomalies. Figure 32 is a map view and Figure 33 is a view from south highlighting the location and extents of different susceptibility bodies.

- Purple anomalies; >0.15 SI.
- Red anomaly; > 0.1 SI and
- Pink anomaly; > 0.06 SI

Susceptibility of 0.06 SI represents the minimum susceptibility measured from the ore samples (green dots). Samples labelled N1 (0.0637 SI) and N2 (0.1657 SI) on Figure 32 represent the lowest and highest susceptibility values of ore samples located within the host rock, olivine-free pyroxenite. These samples are within the mapped ore outlines and are reflected by anomalies D and E, respectively. Two other ore samples (to the top right of anomaly D) were found as boulders at the border of olivine-free rock unit. These samples read 0.3 SI and 0.35 SI. The black dots are locations of other rock samples.

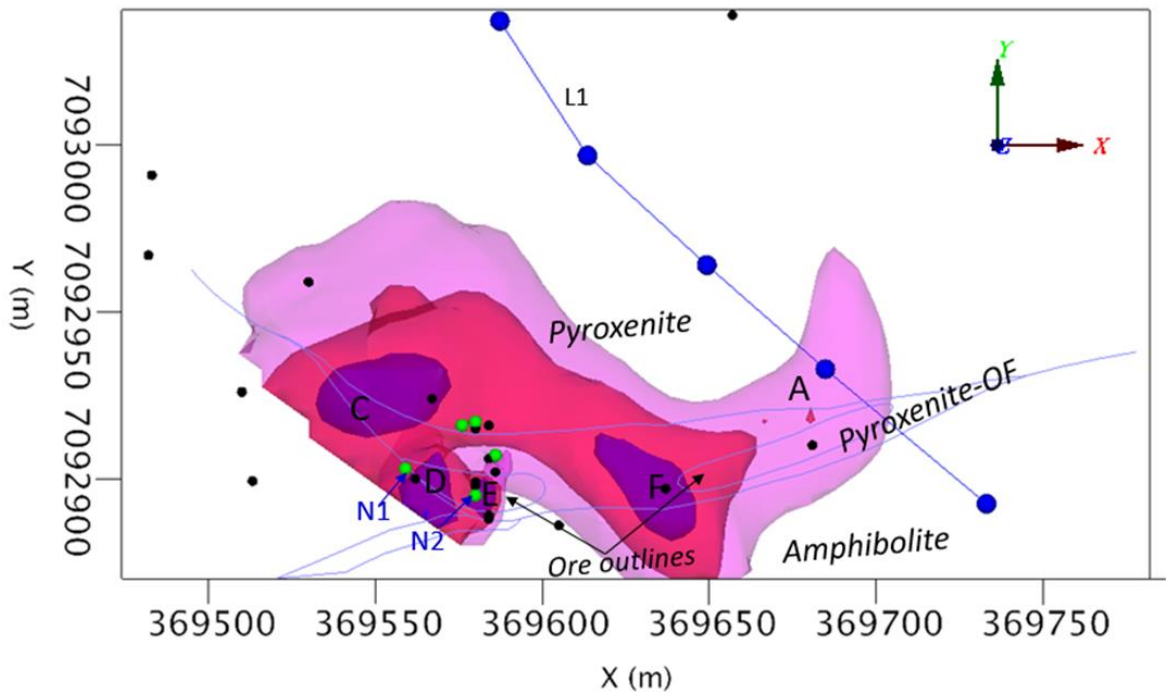

Figure 32: 3D inversion result: Top view at Sucs. > 0.06 SI (Pink), > 0.1 SI (red) and > 0.15 SI (purple). The gravity profile L1 is shown in blue. Geological boundaries are in purple. A-F mark anomalies further explained in the text.

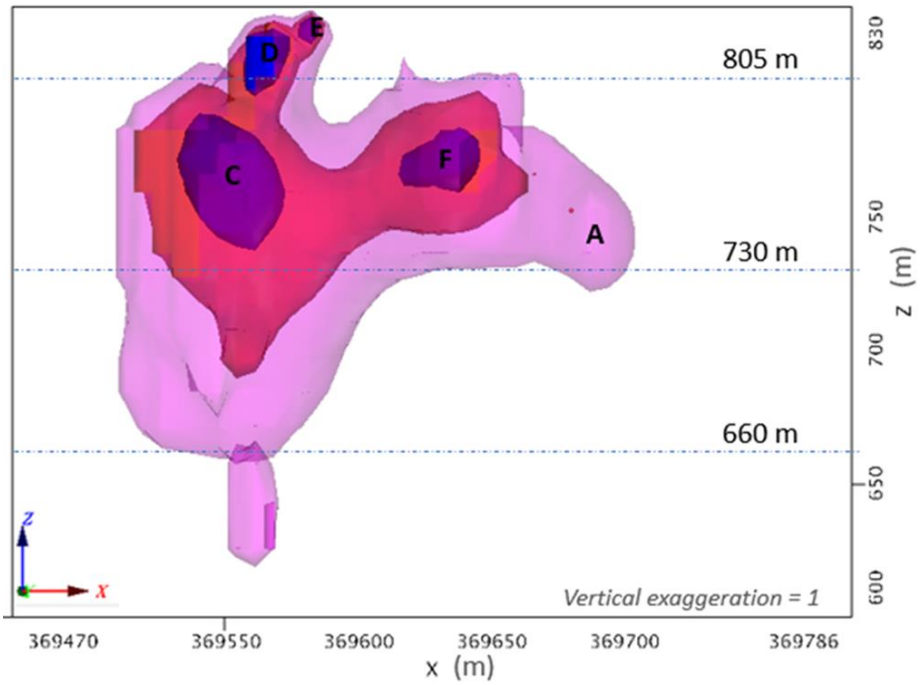

Figure 33: 3D inversion result: View from south at Sucs. > 0.06 SI (Pink), > 0.1 SI (red) and > 0.15 SI (purple). Anomalies D and E are smaller and shallower. A-F mark anomalies further explained in the text.

The interpretation of the prospect is influenced by the results of the 3D inversion. Anomalies A to F vary in shapes and susceptibility magnitude.

- Anomaly A represents the broader high susceptibility body in the area. It is thinner at the tip crossing gravity line L1 and thickens towards the southwest corner (up to145 m thick) where BIF is common.
- Anomalies C to F highlight localised areas of higher susceptibilities within A.
- Anomalies D and E are smaller and shallower bodies directly related to nickel ore samples. Together they make a body of about 30 m thick.
- Anomaly C is about 96 m thick at cut-off >0.10 SI. This anomaly is partly within the olivine-free pyroxenite. The anomaly may be caused by nickel ore or by other magnetic bodies like BIF.
- Anomaly F is about 44 m thick at cut-off >0.10 SI. It is located partly within the olivine-free pyroxenite and at a tip of a mapped ore outline.

To compliment the 3D inversion, the data is interpreted in combination with 2D forward modelling of the ground magnetic and gravity data. The modelling was carried out along three profiles crossing the observed anomalies. The inversion result along the profiles was used as constraint on the anomaly thickness. In areas where the shape and size of the inversion anomaly does not facilitate to fit the data, fitting the observed data becomes preferential over the inversion anomaly. An example is the demarcation of anomaly A in which some locations in the inversion cube have less than 0.06 SI.

The gula schist is the background rock in this area. The base of amphibolite unit was imported from a revised 2D model of line L1, Figure 25. The amphibolite is assigned with susceptibility value of 0.00435 SI and density of 3040 kg/m^3 (Table 1). The reminder of the misfit was fitted by demarcating zones of different susceptibilities on the inversion model and assign different values to fit the observed magnetic data.

Because of relatively high magnetic susceptibilities at the prospect area, the none-ore pyroxenites are fitted at shallow depths.
The results of 2D forward modelling are shown in Figure 34 to Figure 36. There are no acquired gravity profiles along these arbitrary lines. The gravity used for modelling is an extrapolation from line L1 and therefore there is a level of uncertainty.

The ore anomaly on these models is defined by susceptibility values above that of a host rock (0.002 SI) and above 0.0042 SI, the highest value on side rock samples in the area (G1, Figure 29). Density and magnetic properties used for modelling are shown in Table 2.

Table 2: Density and susceptibility values for the ore anomalies

Ore anomaly	A	C	D	E	F
Susc. (SI)	0.06	0.12	0.12	0.12	0.10
Density (kg/m^3)	3000	3250	3250	3250	3250
Remanent: M/I/D	0.5/0/0	1/-30/30	1/-30/30	1/-30/30	1/-30/30

M/I/D stands for magnetization (A/m)), inclination (degree) and declination (degree)

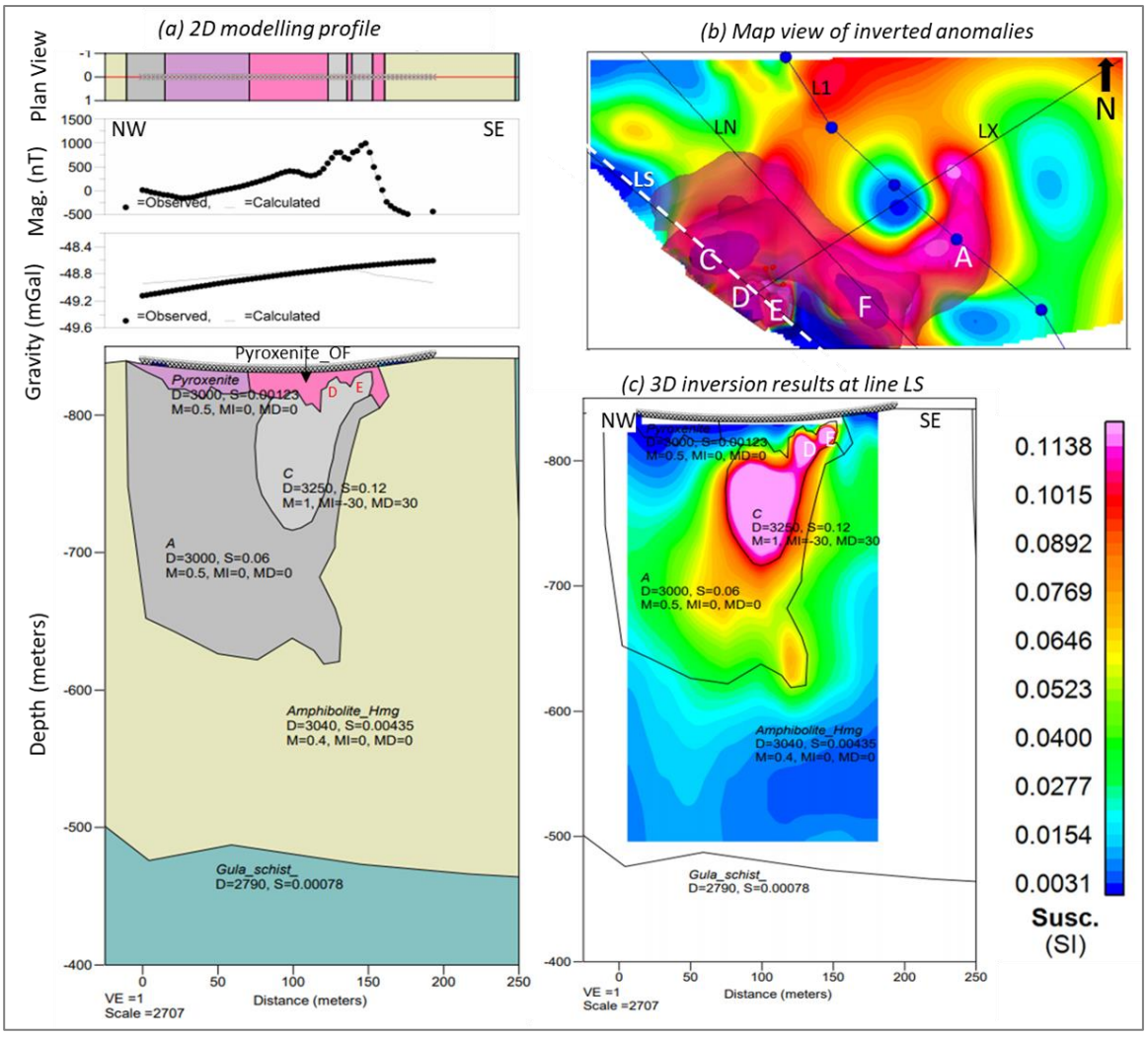

Figure 34: 2D modelling of the nickel ore prospect along the western line, LS. (a) 2D profile with a plan view at (-) 823 m above msl. (b) a map view showing the location of line LS and the respective anomalies overlaying the observed data. (c) 3D inverted model superimposed by 2D model outlines for comparison.

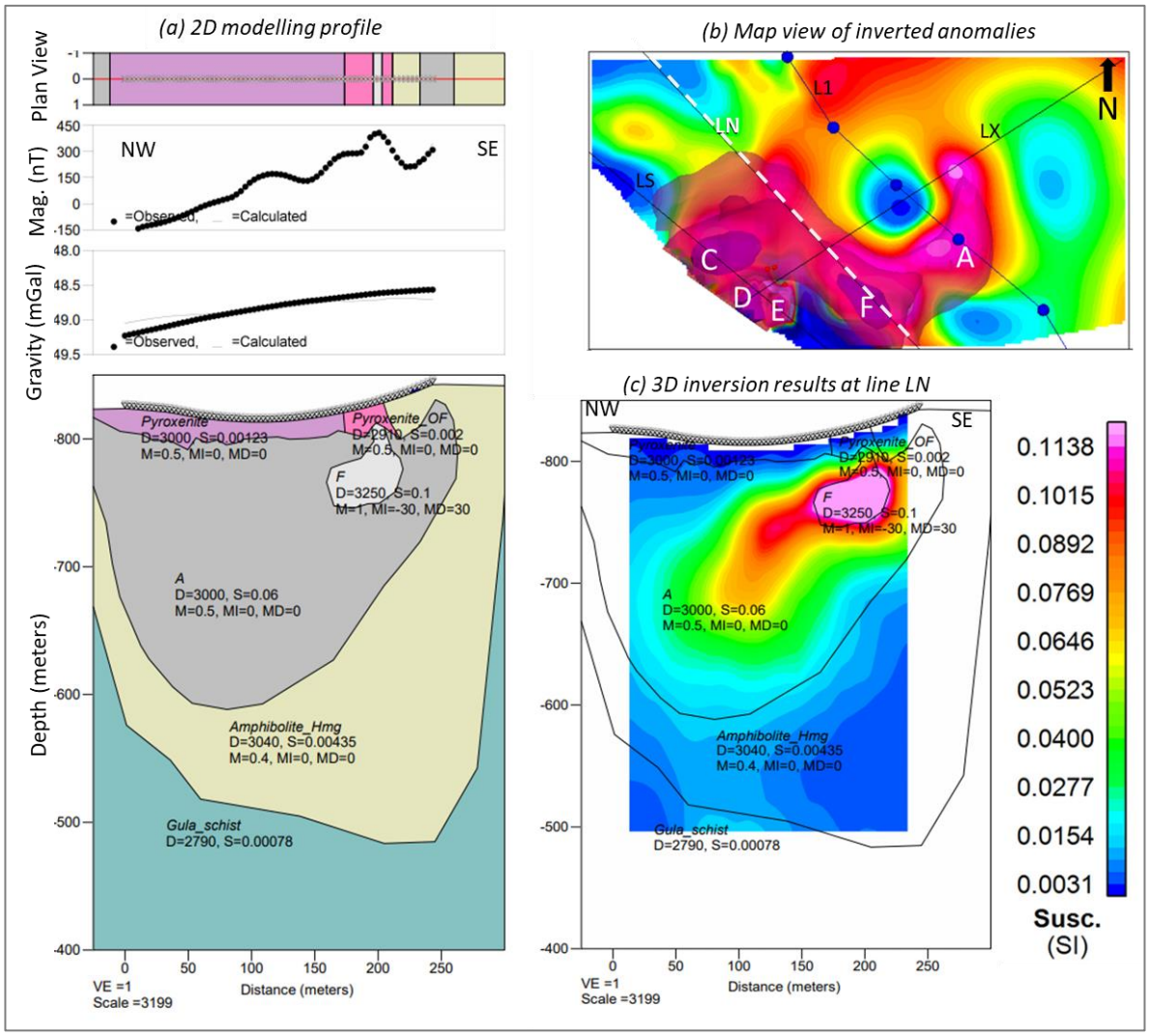

Figure 35: 2D modelling of the nickel ore prospect along the middle line LN. (a) 2D profile with a plan view at (-) 810 m above msl. (b) a map view showing the location of line LN and the respective anomalies overlaying the observed data. (c) 3D inverted model superimposed by 2D model outlines for comparison.

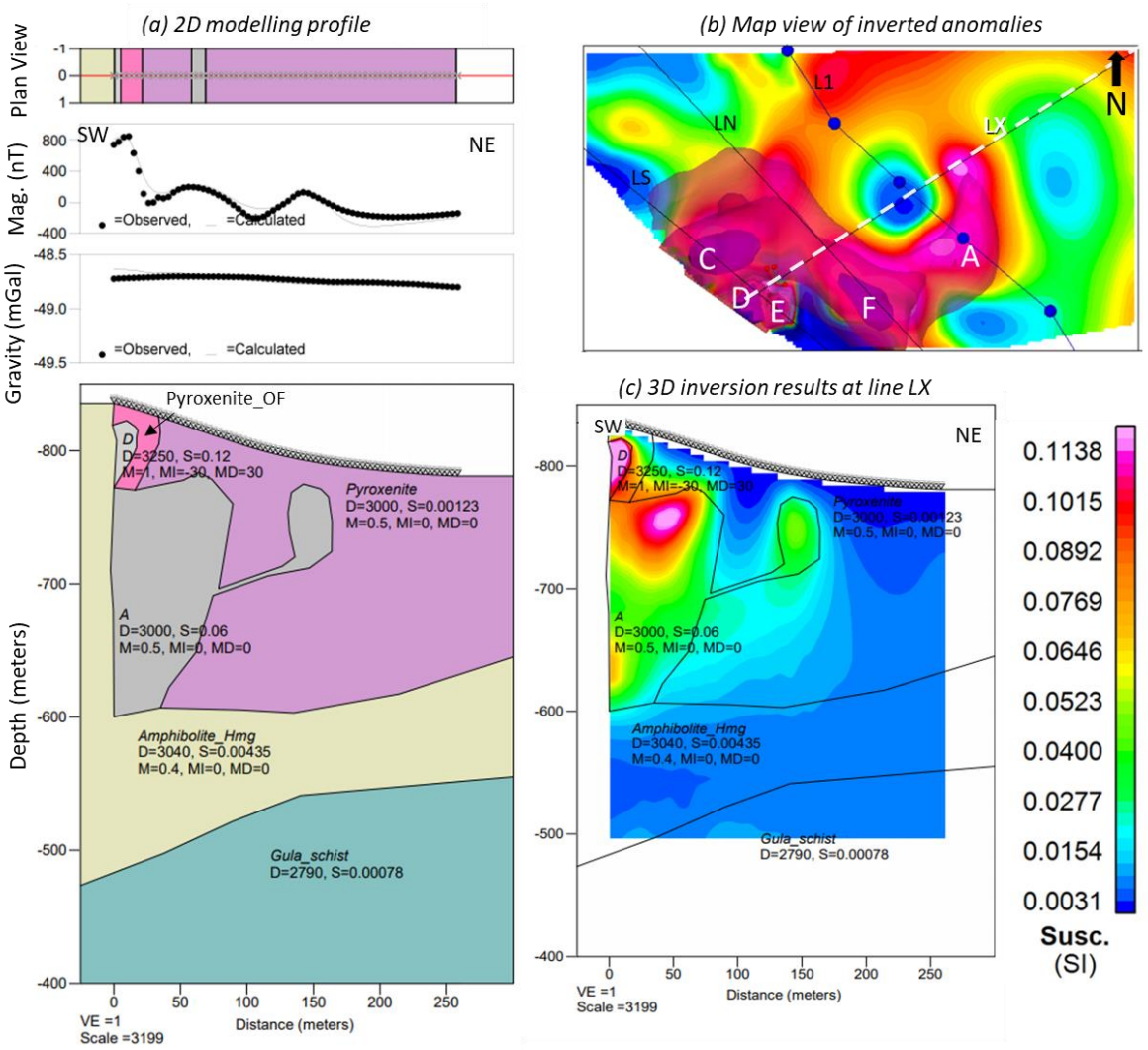

Figure 36: 2D modelling of the nickel ore prospect along the crossing line LX. (a) 2D profile with a plan view at (-) 781 m above msl. (b) a map view showing the location of line LX and the respective anomalies overlaying the observed data. (c) 3D inverted model superimposed by 2D model outlines for comparison.

7. CONCLUSION

2D forward modelling and 3D inversion are the main tools we used for the interpretation of the Brattbakken magnetic data. GM-SYS 2D forward modelling tool can simultaneously model magnetic and gravity data. The two datasets complement each other in seeking a combination of density and susceptibility of a rock type to fit the observed data curves. Availability of gravity profiles along the long lines facilitated the thickness estimation of the intrusions (pyroxenite and gabbro).

3D inversion using VOXI software was done on magnetic data. Background trend removal was applied on input data during inversion to enhance the visibility of localised anomalies while supressing the effect of regional structures. 3D inversion was not carried out for gravity data because the two gravity profiles are too far apart for 3D representation of the prospect area.

Based on the forward modelling and 3D inversion of the airborne data, the intrusions seem to be thicker on line L1 than on L2. The pyroxenite in L1 is about 260 m wide and 270 m thick while on L2 the pyroxenite is about 100 m wide and 120 m thick. The gabbro intrusion on L2 is about 115 m wide and 90 m thick.

At the prospect area an inversion with smaller mesh size was conducted. The results identify four anomalies, C to F with susceptibility of 0.10 SI and above. These anomalies are enveloped in a bigger and relatively lower susceptibility body (0.06 SI) labelled anomaly A. All anomalies are confirmed by 2D modelling.

Anomalies E and D which are about 20 - 30 m thick are directly related to the nickel ore as confirmed by rock samples picked at the location. Anomalies C and F could be caused by nickel ore or other materials. In general, anomaly A which is up to 145 m thick could potentially be a nickel ore body and the susceptibility variations within it indicate differences of ore grades. On the other hand, anomaly A could be any other high magnetic unit. For example, rock sample SKJ 12-24 (0.05358 SI) picked close to anomaly C was identified as sulfide-bearing pyroxenite (Nilsson et al.,2021).

VOXI 3D inversion is newly introduced at NGU and this project is the first to embrace its use as an interpretation tool. The software seems to work well when incorporating some constraints. The confidence in the results so far is backed up by the 2D forward modelling tool which is well-known and uses magnetic and gravity data to complement each other. The inversion of synthetic data provided a guideline on parameter settings although the synthetic data was without added noise.

For a better understanding of VOXI and the survey results, we suggest a study on well-known data from active or inactive mines where ore grading, and production has been performed. This kind of data contain real, observed data uncertainties and hence the results will serve as a benchmark.

8. REFERENCES

Geosoft oasis montaj 9.7.1: gravity processing.

Geosoft oasis montaj 9.8.1: magnetic processing, 2D forward modelling and 3D VOXI inversion.

Geosoft oasis montaj 9.8.1: VOXI Lexicon (geosoft.com).

Li, Y., 2016: 3D Inversion of Magnetic Data Affected by Remanent Magnetization (EAGE E-Lecture, https://www.youtube.com/watch?v=I5qgsZ9Dj-c).

Nilsson, L. P, Paulsen, H-K, Sandstad, J. S, Gellein, J and Mrope, F.M, 2021: Geologiske og geofysiske undersøkellser av Brattbakken Ni-Cu-Co forekomst i Skjækerdalen, Verdal commune, Trøndelag. NGU report nr.2021.016.

Ofstad, F., Dumais, M-A., Tassis, G. and Wang, Y., 2021: Helicopter-borne magnetic, electromagnetic and radiometric geophysical survey in Verdal and Snåsa area, Trøndelag county. NGU report nr. 2021.013.

Scintrex 2019: Scintrex CG-5 Gravity meter. Operation manual. https://scintrexltd.com/wp-ontent/uploads/2017/02/CG5-5-Manual-Ver_8.pdf.

The International Gravity Standardization NET 1971 http://www.sirgas.org/fileadmin/docs/GGRF_Wksp/22_Ruelke_et_al_2019_GGRF.pdf .

Topcon Legacy E 2019: manual.

Wolff, F.C., 1977: Geologisk kart over Norge, berggrunnskart Østersund, M1:250.000. Norges geologiske undersøkelse, Trondheim.

9. APPENDIX

Appendix A1: Maps of magnetic anomalies

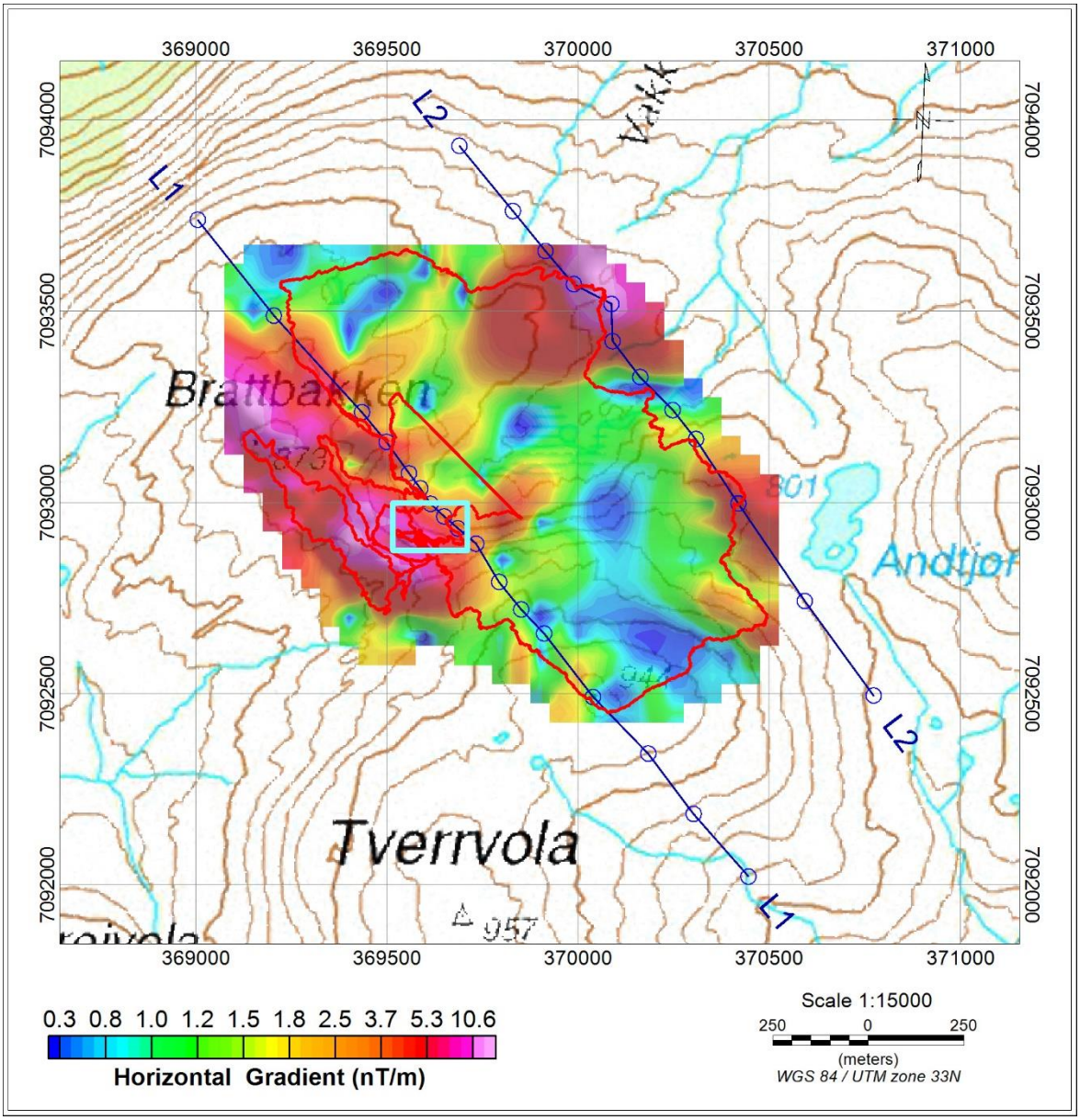

Figure 37: Total Horizontal gradient of the magnetic field at 30% transparent over a relief map. The magnetic profile is shown in red, gravity profiles in blue. The box marks the prospect area.

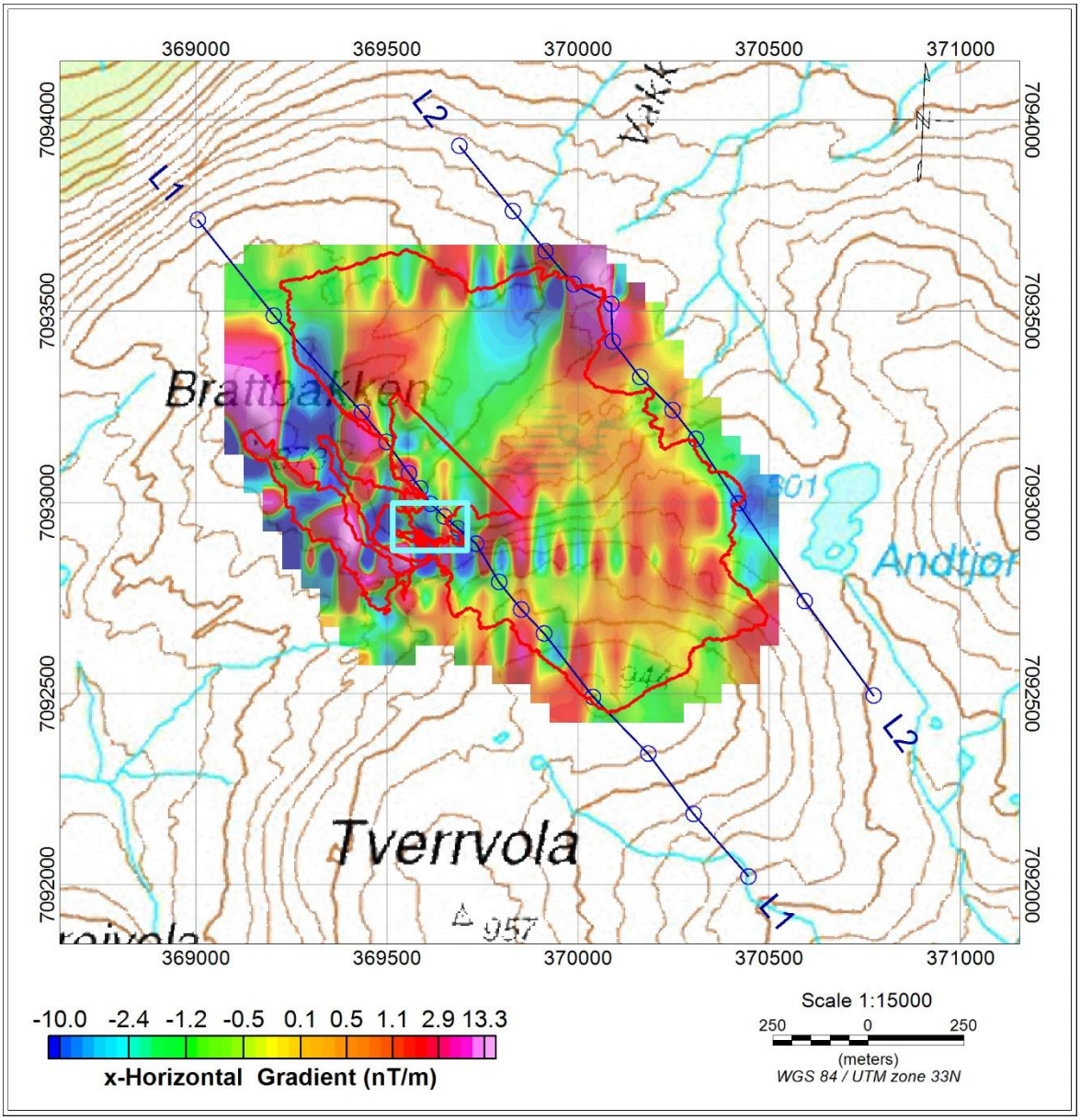

Figure 38: x-Horizontal gradient of the magnetic field at 30% transparent over a relief map. The magnetic profile is shown in red, gravity profiles in blue. The box marks the prospect area.

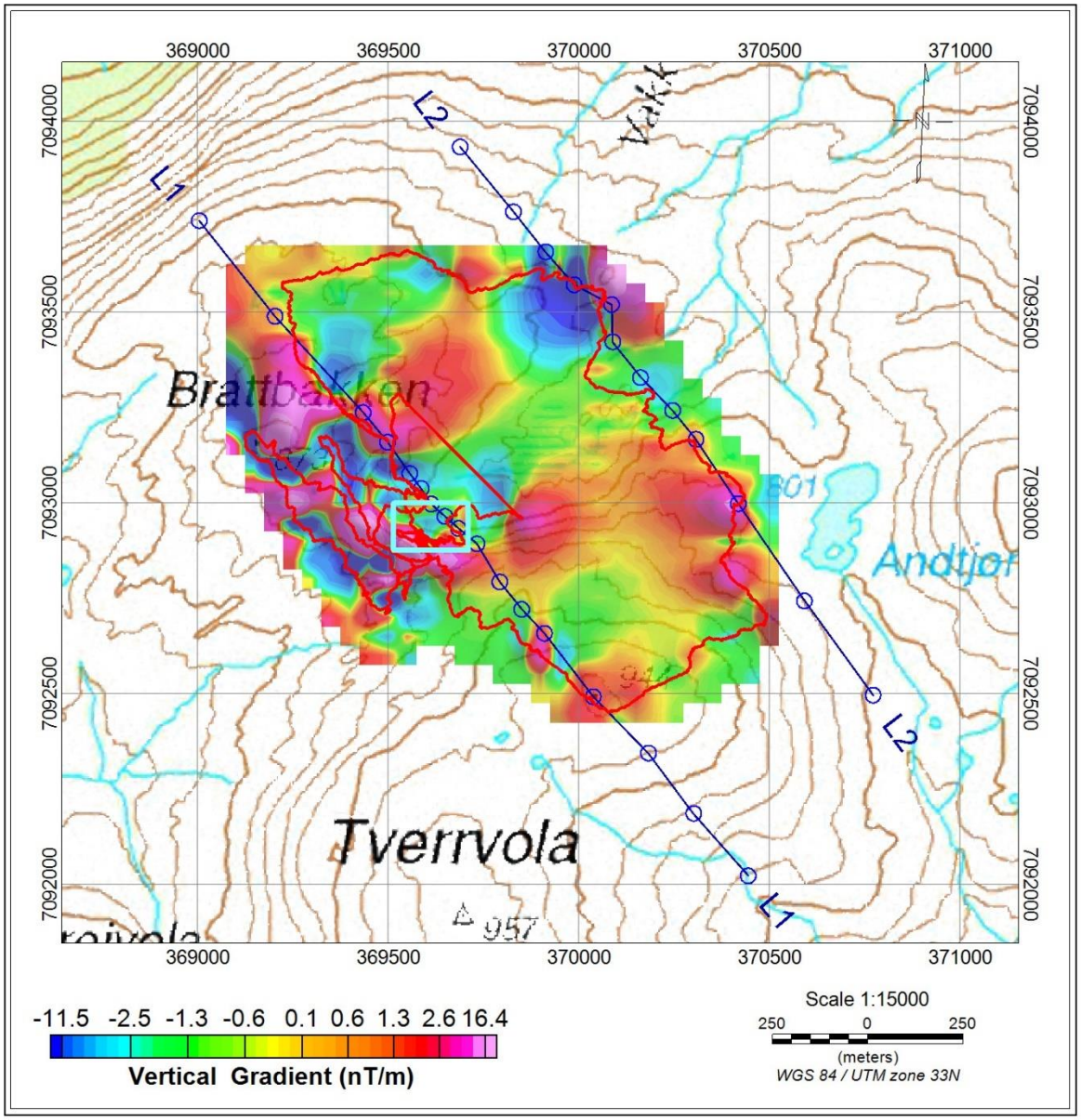

Figure 39: First vertical derivative of the magnetic field at 30% transparent over a relief map. The magnetic profile is shown in red, gravity profiles in blue. The box marks the prospect area.

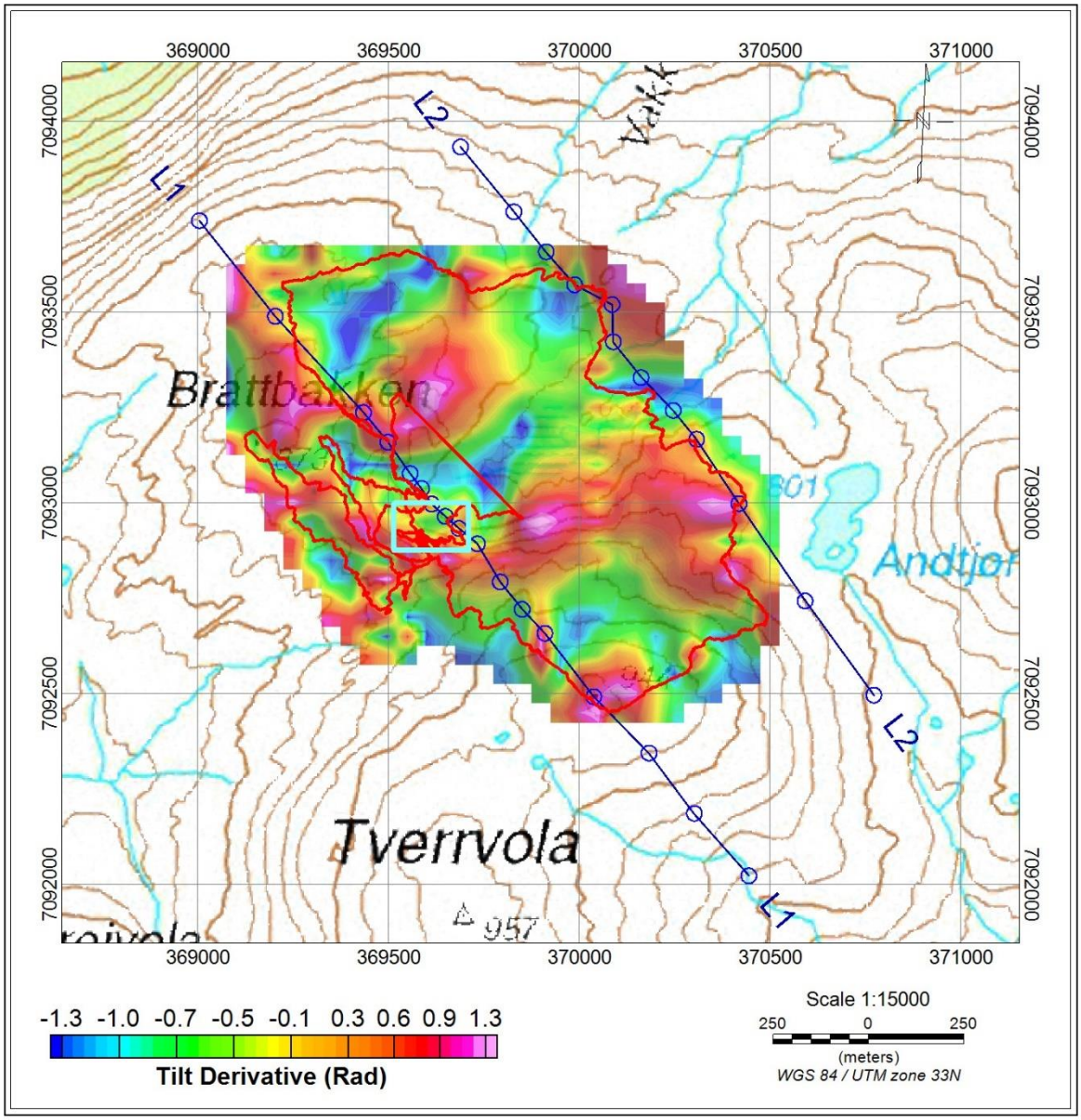

Figure 40: Magnetic Tilt Derivative at 30% transparent over a relief map. The magnetic profile is shown in red, gravity profiles in blue. The box marks the prospect area.

Appendix A2: 2D models down to 14 km deep.

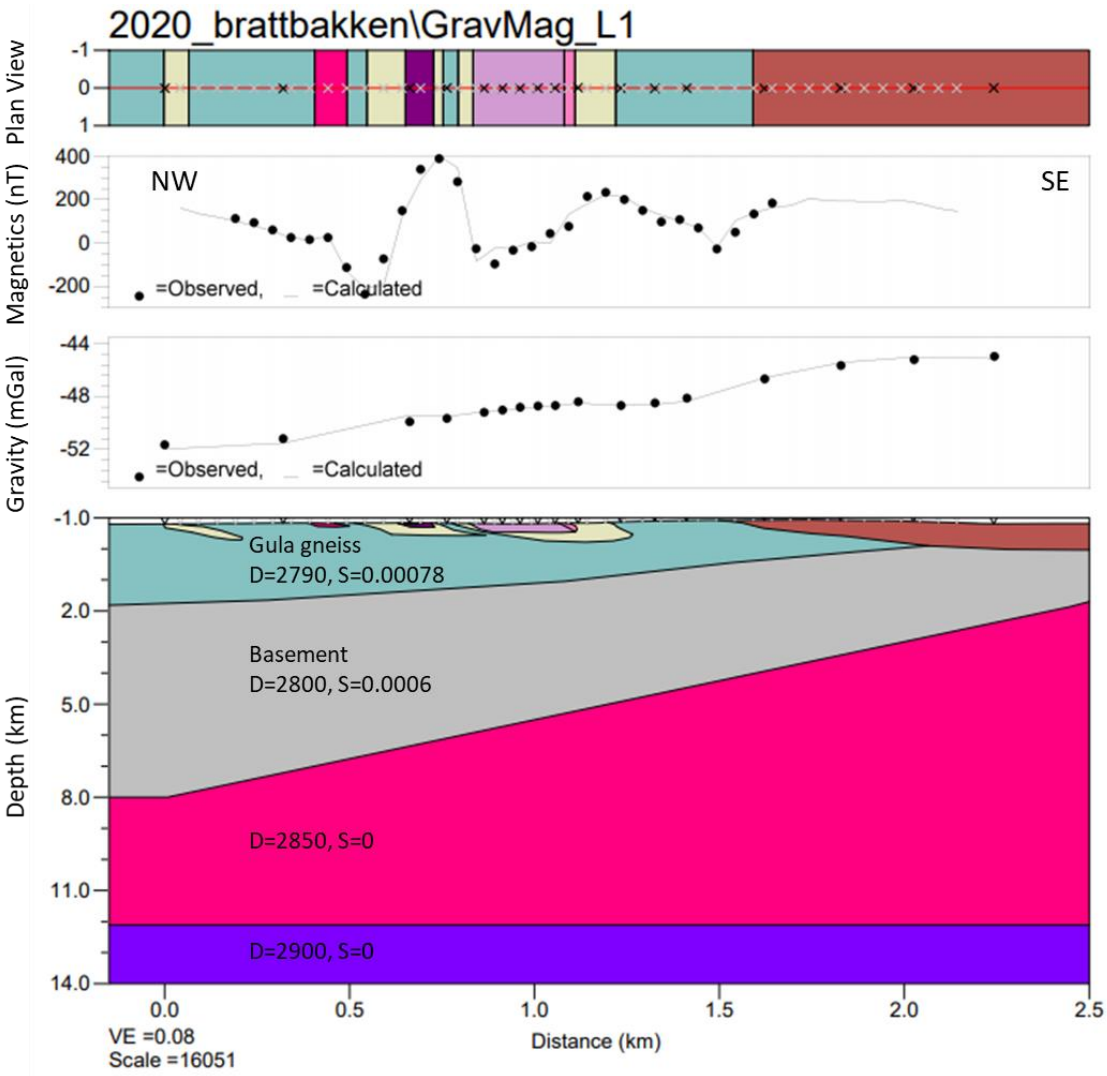

Figure 41: 2D full profile along line L1. The gravity and magnetic profiles in the middle show the calculated (solid lines) and observed data (dots). The plan view is at (-)750 m above msl.

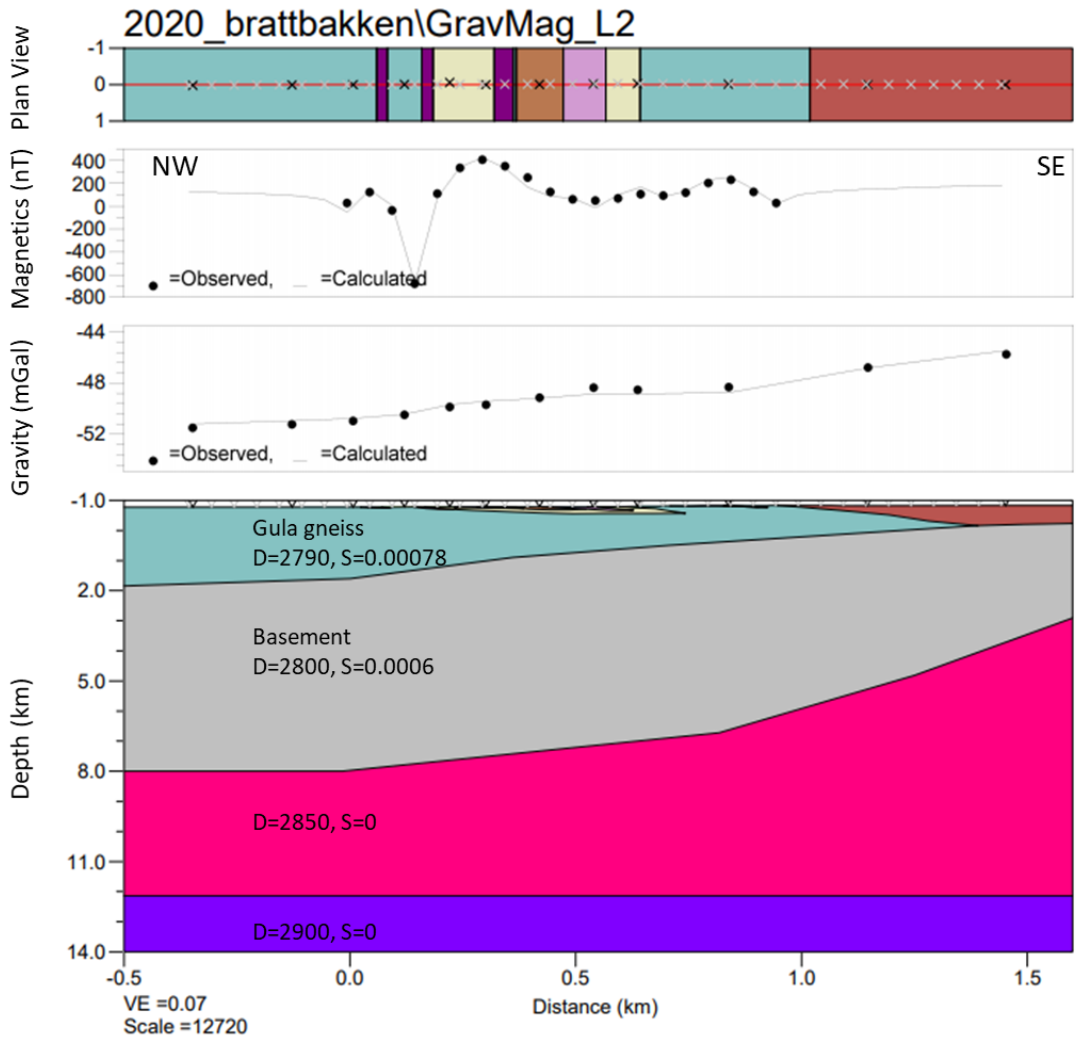

Figure 42: 2D full profile along line L2. The gravity and magnetic profiles in the middle show the calculated (solid lines) and observed data (dots). The plan view is at (-)750 m above msl.

GEOLOGICAL
SURVEY OF
NORWAY

· NGU ·

Geological Survey of Norway
PO Box 6315, Sluppen
N-7491 Trondheim, Norway

Visitor address
Leiv Eirikssons vei 39
7040 Trondheim

Tel (+ 47) 73 90 40 00
E-mail ngu@ngu.no
Web www.ngu.no/en-gb/